Journal Pre-proof

Longitudinal transcriptomic profiling in carrageenan-induced rat hind paw peripheral inflammation and hyperalgesia reveals progressive recruitment of innate immune system components.

Taichi Goto PhD , Matthew R. Sapio PhD , Dragan Maric PhD , Jeffrey M. Robinson PhD , Leorey N. Saligan PhD , Andrew J. Mannes MD , Michael J. Iadarola PhD

PII: S1526-5900(20)30102-4
DOI: https://doi.org/10.1016/j.jpain.2020.11.001
Reference: YJPAI 3892

To appear in: *Journal of Pain*

Received date: 17 July 2020
Revised date: 16 October 2020
Accepted date: 2 November 2020

Please cite this article as: Taichi Goto PhD , Matthew R. Sapio PhD , Dragan Maric PhD , Jeffrey M. Robinson PhD , Leorey N. Saligan PhD , Andrew J. Mannes MD , Michael J. Iadarola PhD , Longitudinal transcriptomic profiling in carrageenan-induced rat hind paw peripheral inflammation and hyperalgesia reveals progressive recruitment of innate immune system components., *Journal of Pain* (2020), doi: https://doi.org/10.1016/j.jpain.2020.11.001

Highlights

- Temporal gene regulatory programs with emphasis on the “inflammatory secretome”
- Sequential waves of leukocytes and antecedent patterns of the chemoattractants
- Subcellular localization of differentially expressed genes providing new targets
- Unique expression patterns of collagen-encoding genes related to tissue remodeling

(i) Title: Longitudinal transcriptomic profiling in carrageenan-induced rat hind paw peripheral inflammation and hyperalgesia reveals progressive recruitment of innate immune system components.

(ii) Short running title: Transcriptomic profiles of peripheral inflammation

(iii) Authors: Taichi Goto[1], PhD, Matthew R. Sapio[2], PhD, Dragan Maric[3], PhD, Jeffrey M. Robinson[4], PhD, Leorey N. Saligan[1], PhD, Andrew J. Mannes[2], MD, Michael J. Iadarola[2], PhD.

(iv) Affiliations

1. National Institutes of Health, National Institute of Nursing Research, Symptom Biology Unit, 10 Center Dr., Bethesda, MD 20892, USA
2. National Institutes of Health, Clinical Center, Department of Perioperative Medicine, 10 Center Dr., Bethesda, MD 20892, USA
3. National Institute of Neurological Disorders and Stroke, Flow and Imaging Cytometry Core Facility, 10 Center Dr., Bethesda, MD 20892, USA
4. University of Maryland, Baltimore County, Translational Life Science Technology Program, 1000 Hilltop Cir., Baltimore, MD 21250, USA

(v) Corresponding author

Michael J. Iadarola, PhD

Department of Perioperative Medicine, Clinical Center

Building 10, Room 3D56, 10 Center Drive, MSC 1510

National Institutes of Health

Bethesda, MD 20892-1510

Office: 301-496-2758

michael.iadarola@nih.gov

(vi) Disclosures

This study was supported by the Division of Intramural Research Program of the National Institute of Nursing Research, the Department of Perioperative Medicine, Clinical Center and the National Institutes of Neurological Disorders and Stroke, National Institutes of Health. Supplemental

funding was provided the National Center for Complementary and Integrative Health, and from the Office of Behavioral and Social Science Research.

We have no conflict of interest to declare.

Abstract

Pain is a common but potentially debilitating symptom, often requiring complex management strategies. To understand the molecular dynamics of peripheral inflammation and nociceptive pain, we investigated longitudinal changes in behavior, tissue structure, and transcriptomic profiles in the rat carrageenan-induced peripheral inflammation model. Sequential changes in the number of differentially expressed genes are consistent with temporal recruitment of key leukocyte populations, mainly neutrophils and macrophages with each wave being preceded by upregulation of the cell-specific chemoattractants, *Cxcl1* and *Cxcl2*, and *Ccl2* and *Ccl7*, respectively. We defined 12 temporal gene clusters based on expression pattern. Within the patterns we extracted genes comprising the inflammatory secretome and others related to nociceptive tissue remodeling and to sensory perception of pain. Structural tissue changes, involving upregulation of multiple collagens occurred as soon as 1-hour post-injection, consistent with inflammatory tissue remodeling. Inflammatory expression profiling revealed a broad-spectrum, temporally orchestrated molecular and cellular recruitment process. The results provide numerous potential targets for modulation of pain and inflammation.

Perspective

This study investigates the highly orchestrated biological response during tissue inflammation with precise assessment of molecular dynamics at the transcriptional level. The results identify transcriptional changes that define an evolving inflammatory state in rats. This study provides foundational data for identifying markers of, and potential treatments for, inflammation and pain in patients.

Key words

Transcriptome, carrageenan, peripheral inflammation, temporal gene expression pattern, differentially expressed gene, pain, RNA sequencing, secretome, chemokine, cytokine, interleukin, collagen, neutrophil, macrophage

Introduction

Pain is a common yet complex and potentially debilitating symptom that can negatively influence the quality of life for patients with acute and chronic medical conditions.[56] In the United States, approximately 100 million adults are affected by chronic pain at a total medical cost of approximately $600 billion in 2010.[13] Providing appropriate pain management with accurate pain assessment in the early phases of tissue injury is essential. However, difficulties in accurately assessing pain can be encountered due to complexities associated with the etiology of the original insult and the neural mechanisms of nociception that are activated. Therefore, understanding the mechanisms and identifying biomarkers of pain by unraveling the trajectory of the pain process from its origin in peripheral tissue through to transmission to the spinal cord can contribute to the development of new therapeutic strategies to improve the assessment and management of pain.

The first steps in the pain pathway often involve peripheral tissue damage and inflammation. The present paper uses a data-driven approach to examine the molecular events that unfold during an experimental inflammation occurring in the hind paw of a rat. The inflammation was induced by intraplantar λ-carrageenan, a sulfated polysaccharide isolated from red alga *Chondrus crispus*.[36] It basically acts as a xenobiotic mimetic of a foreign agent. Carrageenan is frequently used to produce a persistent pain state characterized by behavioral hyperalgesia, allodynia other pain behaviors. While sensitized behaviors and accompanying central gene and physiological alterations in spinal cord dorsal horn have been examined,[47] the peripheral microenvironment that may contribute to the hyperalgesic state requires more in-depth molecular investigation. Here we performed a fine-grained temporal analysis of gene regulatory programs that occur in the inflamed rat hind paw and algesic behavioral changes following carrageenan injection. A dynamic evolution of multiple gene profiles was observed over the course of the inflammatory hyperalgesia and allodynia. The process involves locally induced transcripts comprising an “inflammatory secretome” that

orchestrates two main waves of leukocyte migration: an early neutrophil infiltration and a later recruitment of macrophages. The mRNA sequence data provides detailed transcriptomic profiling of peripheral tissue contributions to both the initiation of pain onset and sustained inflammation following tissue damage. Many of the identified factors provide new insight into novel or partially characterized pathways and may lead to the identification of pain biomarkers and new candidate therapeutic targets to be tested.

Materials and methods

Animal care and carrageenan inflammation

Experiments were approved by the Institutional Animal Care and Use Committee of the Clinical Center, National Institutes of Health (Bethesda, Maryland). Animals were cared for and tested in accordance with ethical guidelines established in the NIH Guide for Care and Use of Laboratory Animals. Male Sprague Dawley rats (200 to 300g) were housed in pairs with 12-hour light-dark cycles, fed ad libitum, and were tested and monitored for behavior during the animal's light cycle. Animal cages were furnished with a plastic tunnel for enrichment. Acute inflammation was induced in male Sprague Dawley rats by injecting freshly prepared 4% (W/V) of carrageenan in 0.9% sterile saline into the left hind paw. Animals were euthanized at 0 (naïve), 1, 4, 8, 24, 48, and 72 hours after the injection, and hind paw tissues were harvested for next-generation RNA sequencing and histological analyses. We used four to six rats for hind paw thickness measurement and behavioral tests, and three rats for RNA sequencing and three for histology for each timepoint.

Hind paw edema evaluation and behavioral tests

Hind paw edema was evaluated by measuring dorsoventral hind paw thickness using a caliper. Thermal hyperalgesia was detected by the Plantar Test Instrument (Ugo Basile, Comerio, Italy). Unrestrained rats were placed on a glass platform under a plastic enclosure for at least five minutes for habituation. Then, the lamp was positioned under the paw and thermal stimulation applied until paw withdrawal occurred. The assay was stopped at 25 s if no withdrawal occurred. Mechanical allodynia was detected using calibrated von Frey monofilaments. Animals were placed on an elevated wire mesh surface, and monofilaments of increasing

bending force were applied to the plantar surface of hind paws until two consecutive withdrawals for a particular filament were observed or 60 g (the cutoff value) was reached. Then monofilaments of decreasing strength were applied until consecutive withdrawals were not observed. The up-down method was continued until the thresholds became consistent. If no withdrawal response was observed, the cutoff value of 60 g was recorded. Pin-prick test was used to assess guarding behavior as a measure of mechanical hyperalgesia. The plantar surface of the hind paw was touched with the point of a safety pin at an intensity sufficient to produce a reflex withdrawal response.[5] The paw withdrawal duration (guarding) was recorded in seconds and the normal quick reflex withdrawal response was given the value of 0.5 s. The hind paw thickness and behavioral tests were analyzed using repeated-measures two-way ANOVA with Sidak's post-hoc multiple comparison method.

RNA extraction, library preparation, and next-generation sequencing

RNA extraction was performed from flash frozen hind paw tissue using a Fastprep 24 and lysing matrix D (MP Biomedicals, Santa Ana, CA), and Qiazol (Qiagen) followed by the RNeasy miniprep kit as described previously.[26] Library preparation and sequencing were performed by the NIH Intramural Sequencing Center using PolyA+ selection and unstranded library preparation.[41, 46] Libraries were constructed from 1 µg mRNA using the Illumina TruSeq RNA Sample Prep Kits, version 2. The resulting cDNA was fragmented using a Covaris E210 ultrasonicator. Library amplification was performed using 8 cycles to minimize the possibility of over-amplification. Unique barcode adapters were applied to each library. Libraries were pooled in equimolar ratio and sequenced together on a HiSeq 2000 with ver 3 flow cells and sequencing reagents. At least 34 million 100-base read pairs were generated for each individual library. Data were processed using RTA 1.12.4.2 and CASAVA 1.8.2.

Alignment, quantification, and statistical analyses of RNA sequencing data

Alignment from raw read data was performed using MAGIC software and a Rn6 genomic target with RefSeq annotations.[26, 41] The MAGIC pipeline uses significant fragments per kilobase million (sFPKM) as a unit of abundance. The calculation for sFPKM estimates the expression level from read counts to limit the

influence of protocol biases as described previously.[62] Briefly, this measure corrects for several sources of distortion such as transcript length, GC content, library sequencing depth, genomic contamination, and insert size. For representation throughout the manuscript, we show gene changes in terms of expression ratio. In this calculation, we smooth the effects of dividing by small numbers by adding a small number (0.1) to both the numerator and denominator using the following formula:

$$Expression\ ratio = \frac{sFPKM\ (each\ timepoint) + 0.1}{sFPKM\ (untreated\ control) + 0.1}$$

Differentially expressed genes (DEGs) are identified by comparing the distributions of gene expression of each gene across two sample groups of timepoints in both directions individually. This analysis is part of the MAGIC pipeline, and is performed using default parameters as described previously.[26] Briefly, each gene is given a DEG score in the range 0 to 200, where 200 indicates a gene which separates perfectly between the two groups examined. A threshold is chosen by controlling the false discovery rate (FDR) to no more than 5%. As an additional consideration, in some cases the FDR is automatically selected lower than 5% in cases where the addition of more genes would exceed an incremental FDR of 20%. This occurs in situations where there is a population of high confidence DEGs with very low FDR calculations, where the addition of additional DEGs to reach an average value of 5% adds genes with low confidence estimates. Detailed statistical methods and validation of these techniques have been reported previously.[26, 62]

Classification of subcellular compartment among differentially expressed genes

We assorted genes into five exclusive categories based on the major subcellular location of the mature protein: secreted, extracellular structural proteins, plasma membrane, cytoplasm, and nucleus. Uncategorized/other genes are reported as a sixth category. This classification was performed based on data from the following databases: Uniprot [55], LocDB [42], COMPARTMENTS [4], and Human Protein Atlas (http://www.proteinatlas.org) [53], all of which are publicly available. Data on subcellular localization of all genes were extracted from each of these databases and examined. Due to the lack of a cohesive labeling schema throughout these four databases, the information was generally harmonized manually to conform to the six categories. A small number of genes did not match within any of the databases and were classified manually

based on literature searching. In cases where a discrepancy was observed between datasets, this was generally resolved manually by considering the descriptions in each of these databases, and additional information from the literature as needed.

Hierarchical clustering and heatmap generation

To cluster genes based on the expression patterns, hierarchical clustering and heatmap visualization were performed using sFPKM values. Before plotting in the heatmap, expression was transformed by dividing each value by the maximum sFPKM for that gene across the time course, with resulting in values between 0 and 1. DEGs between any two timepoints were used to construct a heatmap based on ratios of expression between timepoints, representing the time course of gene expression. The heatmap data were clustered using the dist (Euclidean) and hclust (ward.d2) functions in R and plotted using heatmap·2 with viridis "inferno" coloration. Twelve branches of the dendrogram were considered to break the gene expression patterns into groups. We evaluated whether one cluster was a subset of an adjacent cluster if there was no significant difference in the proportion between the two clusters by chi-square test (Table S1). As a result, for the subcellular localization graphs, Cluster F was defined as a subset of Cluster E and they are treated together. Similarly, Cluster H and I are treated together.

For heatmaps with smaller numbers of genes, expression was transformed by dividing each value by the maximum sFPKM for that gene across the time points, resulting values between 0 and 1, and ratios are plotted for each gene relative to maximum expression. These heatmaps were created by Microsoft® Excel for Mac 16.16.18 and sorted by peak expression in the time course, and then secondarily sorted by max sFPKM value. The yellow, white, and purple colors indicate 1, 0.5 and 0, respectively.

Histological analyses

Animals were deeply anesthetized and perfused intracardially with cold phosphate buffered saline followed by 4% paraformaldehyde. Hind paw tissue was dissected and post-fixed in 4% paraformaldehyde for a minimum of 16 hours but not more than 36 hours. Samples were embedded in paraffin blocks and 6 μm

sections were mounted by Histoserv Inc. (Germantown, MD). Hematoxylin and eosin staining and Masson's trichrome staining was performed using a standard methods. Masson's trichrome staining stains keratin and muscle fibers in red, collagen and bone in blue, cytoplasm in pink, and cell nuclei in dark brawn.

Multiplex *in situ* hybridization was conducted using the RNAscope® Multiplex Fluorescent assays v2 (Advanced Cell Diagnostics, Newark, CA) with Tyramide Signal Amplification (Opal™ Reagent Systems; Perkin Elmer, Waltham MA). Stained sections were imaged on an Axio Imager.Z2 slide scanning fluorescence microscope (Zeiss, Oberkochen, Germany) equipped with a 20X/0.8 Plan-Apochromat (Phase-2) non-immersion objective (Zeiss), a high-resolution ORCA-Flash4.0 sCMOS digital camera (Hamamatsu, Shizuoka, Japan), a 200W X-Cite 200DC broad band lamp source (Excelitas Technologies, Waltham MA) and 5 customized filter sets (Semrock, Rochester NY) optimized to detect the following fluorophores: DAPI, Opal520, Opal570, Opal620, Opal690. Image tiles (600 × 600 mm viewing area) were individually captured at 0.325 micron/pixel spatial resolution, and the tiles seamlessly stitched into whole specimen images using the ZEN 2 image acquisition and analysis software program (Zeiss), with an appropriate color table applied to each image channel to either match its emission spectrum or to set a distinguishing color balance. Pseudocolored stitched images were overlaid as individual layers to create multicolored merged composites.

The images were processed by Adobe Photoshop and 20.0.0 and ImageJ 2.0.0-rc-69/1.52p to analyze co-localization of detected genes in the multiplex *in situ* hybridization images.

Immune cell and pathway analysis with the Imsig R package

We used the Imsig R package to estimate relative immune cell abundance at each timepoint. Imsig tests for co-expression of several dozen cell-type specific (or primarily cell-type specific) genes to develop a relative score for immune cell type abundance (and biological pathway activity including interferon, proliferation, and translation) in heterogenous tissue. Imsig has been shown to perform favorably against other algorithms using similar approaches. The Imsig paper and the software repositories (CRAN and GitHub) provide complete gene lists used for score determination, and further detail on how scores are calculated.[37] Imsig was developed for analysis of tumor immune microenvironment, here we show that it provides results consistent with canonical

patterns of inflammatory induction/resolution in this rat cutaneous tissue model as well. Implementation of the Imsig package in this study is described in a new GitHub repository (https://github.com/PhyloGrok/AnalyzeComplexTissues), with the processed data and R-code used for this analysis provided open-source (pending publication).

Results

Analysis of the RNA sequencing results yielded 3,817 genes that were differentially expressed in at least one of the timepoints examined. We excluded a total of 897 uncharacterized genes. The remaining 2,920 characterized genes were analyzed further.

Carrageenan-induced hind paw inflammation and DEGs

Edema, thermal hyperalgesia, and mechanical allodynia and hyperalgesia were evident within 1 hour after carrageenan injection and were sustained at least for 72 hours (Figure 1A–D).

After carrageenan injection, the papillary structure became flattened and the epidermal layer became thickened. Abundant potentially induced resident and infiltrating leukocytes were observed commencing at 4 hours and were further increased between 8 and at least 72 hours after carrageenan injection as shown in the histological time course montage (Figure 1E–K, low-power images on the left and higher magnification images on the right). The stratum corneum started to peel off at 24 hours. The panels in Figure 1L–Q show graphical overviews of the differentially-induced and -suppressed genes at each time point with several examples indicated in each panel. The majority of the alterations were elevations in gene expression although there were clear contingents of genes undergoing suppressed expression.

Examination of the most highly and rapidly induced genes

The genes that underwent the greatest differential induction compared to untreated controls were *Il6* (interleukin 6) and *Ccl12* (C-C motif chemokine ligand 12); their expression ratios were 199 and 183, respectively (Table 1). The most rapidly induced genes were *Cxcl1* (C-X-C motif chemokine ligand 1) and

Cxcl2 (C-X-C motif chemokine ligand 2) which act as neutrophil chemoattractants[10] and were induced within one hour of injection (Figure 2A). A second set of chemokines, including the monocyte and macrophage chemoattractants, *Ccl2* (*Mcp1*) and *Ccl7*[1, 40] showed a later peak at 4 hours post-injection. Anatomical analyses localize select genes in this group to specific cell populations in the inflamed hind paw (Figure 2B–I, see also Figure 3). *Cxcl1* and *Cxcl2* were mainly found in leukocytes but we found several signals at nerve bundles (Figure 2B and C). *Il6* and *Cxcl10* were strongly expressed at vascular cells (Figure 2D–G).

Major components of infiltrating immune cells

We next focused on the peripheral targets of chemoattractants using cell-type-specific markers. When considering the total number of up- and down-regulated genes (Bars, Figure 3A), we observed two peaks of expression, one at 8 hours and one at 48 hours, which are consistent with tissue infiltration of neutrophils and macrophages, and appearance of *S100a8/a9* and *Cd68*, markers respectively.[19, 57] A bioinformatic analysis using the Immune Cell Gene Signatures (imsig) package for R also supports this result (Figure S1) and discloses a small increase in B-cell signal at late timepoints as well. Indeed, this analysis showed transcriptional signatures suggesting relative increases of NK cells (NK signal being quite small, but observable), T-cells, and monocytes during the 24- to 72- hour timepoints. This analysis is based on signatures of each of these infiltrating immune cells and is designed to work in tissue transcriptomics where immune cell infiltration is observed. Interestingly, *in situ* hybridization for *S100a9* revealed a prominent second site of regulation, the keratinocyte layer (Figure 3B and C), in addition to scattered cells in subcutaneous tissue (Figure 3D and E). At 48 hours, *Cd68*-expressing cells were found throughout the inflamed tissue with the exception of epidermis and muscle tissues (Figure 3F, G, and S2).

Gene expression clusters according to temporal patterns and degree of induction

The DEGs were classified by temporal expression into 12 distinct clusters (Figure 4A). Because of their overall closeness and similarity, clusters F and E, and H and I were treated together (Table S1). The full gene sets are in Tables S2–S11. Figure 4B, C, and Table S12 show the numbers and proportions of induced or

recruited genes according to subcellular location mapping: secreted, matrix and other extracellular proteins, plasma membrane, cytoplasmic, nuclear, and additional genes. Cluster C, which represents the very early (1 to 4 hours post-injection) up-regulated transcriptional responses, had 27% of its genes in the secreted category, and this cluster contained the largest proportion of secreted genes among all the clusters (Table S12).

Figure 5A shows the 50 genes exhibiting the highest expression ratio in Cluster C (peak at 1–4 hours, full list in Table S4). Figure 5B–I show localizations of representative genes in the cluster. Of the 50 genes, in the untreated control, there were 16 that were expressed at less than 1.00 sFPKM (e.g., *Cxcl2* and *Cxcl1*), 19 that had expression ranging from 1.00 to less than 10.00 sFPKM (e.g., *Apold1* and *Atf3*), and 15 that had expression levels of 10 or more sFPKM (e.g., *Ctgf*, *Nr4a1*, *Cyr61*, and *Errfi1*). We use timing and the sFPKM range to distinguish genes for which expression is induced in resident cells in the inflamed tissue compared to genes expressed in cells that enter the tissue because of recruitment from the vascular compartment. For example, the expression of *Cxcl2* was increased from 0.16 at baseline to a peak of 27.6 by 1 hour. This gene colocalized to cells located in the interstitial spaces of the hind paw (Figure 2C and 5C–E). The rapid induction immediately after injection suggests that these genetic changes are occurring in resident cells in the tissue rather than in cells recruited from the vasculature. On the other hand, the expression level of *Atf3* (activating transcription factor 3, a leucine zipper transcription factor) changed from 5.1 to 50.8, and the expression occurred in in the keratinocyte cell layer (Figure 5G). This suggests that basal-state keratinocytes constitutively express a low level of *Atf3*, which is enhanced during the early stages of carrageenan inflammation. For the *Errfi1* (ERBB receptor feedback inhibitor 1, a negative regulator of EGFR signaling involved in keratinocyte proliferation), the expression changed from 17.4 to 112.2 and expression was localized to the keratinocyte (Figure 5G), subcutaneous layers, and leukocytes (Figure 5I) consistent with up-regulation and recruitment. The diversity of affected cell types suggests that, at this time segment, elevated transcription is contributed by enhanced expression in resident cells with some proportion of transcripts contributed by early infiltrating leukocytes[38] To obtain a better understanding of the cell populations, we examined colocalizations of positive signals for four genes using *in situ* hybridization (Figure 5J–M). Approximately 50% of *Cxcl2* positive cells

also expressed *Cxcl1* but only 30% of *Cxcl1* positive cells expressed *Cxcl2*. Other pairs of genes exhibited a range of coexpression from a low of 5% (*Cyr61* + *Cxcl2*) and up to 33% (*Cxcl2* + *Apold1*).

Inflammatory secretome

To determine key regulators of intercellular communication in this inflammatory model, we examined genes encoding secreted peptides and proteins, the "secretome." Table 2 and Figure 6A indicate the 50 genes exhibiting the highest expression ratio and examples of high expressors were found in all the time epochs (Figure 6A–D). Many of the inflammatory secretome DEGs were transcripts coding for chemokines or cytokines. The most differentially expressed chemokine or cytokine genes were *Cxcl2* in Cluster C, *Cxcl10* in combined Cluster E-F, *Il6* in Cluster G, *Ccl12* in combined Cluster H-I, and *Ccl3* in Cluster J. Figure 6B,C shows the representative genes encoding cytokines and chemokines that have more than 10 sFPKM as the maximum value. Of the top 50 genes, only 4 had a basal expression level of more than 10 sFPKM (*Ccl2*, *Cfb*, *Ctsz*, and *Timp1*). The remainder of the secreted protein-encoding genes with low basal expression may be expressed by recruited cells that infiltrate the tissue from the vasculature. Interestingly, some genes with elevated expression at an early point went down to the baseline later in the time course. In addition to the familiar cytokines and chemokines, several other types of peptides or proteins were represented in the secretome. These include proteases and protease inhibitors: two members 1 and 4 of the *Adamts* family (ADAM metallopeptidase with thrombospondin), *Ctsz* (cathepsin Z), two members of the *Mmp* family of metalloproteinases and their inhibitor, *Timp1*, and the serine proteinase inhibitor *Serpine1*. Figure 6D shows those genes encoding proteases and their inhibitors that have more than 10 sFPKM at the maximum value. Although levels were low, we also detected upregulation of the intercellular linking molecule Cerebellin 1, *Cbln1*, which is highly expressed in the cerebellum but also in DRG.[16] Together, these secreted molecules can shape the tissue response in terms of intercellular signaling, matrix remodeling, and hyperalgesia. The full dataset of the inflammatory secretome is presented in Table S13.

Tissue remodeling

Masson's trichrome staining of dermis layers at different time-points after treatment is shown in Figure 7A–F. From 4 hours after treatment, lacunae developed in the dermis (black arrows in Figure 7B and C). Subsequently, neovascularization was observed at 24 through 72 hours, (yellow arrows in Figure 7D–F). These results suggest that the dermal collagen structure is disrupted during the carrageenan inflammatory response, inducing tissue remodeling that is supported by an underlying broad transcriptional response. While many collagen genes were expressed at baseline (Figure 7G), three genes related to tissue remodeling, *Cthrc1*, *Il1a*, and *Ctgf*, were rapidly induced at 1 hour (Figure 7G). They encode collagen triple helix repeat-containing 1, interleukin 1 alpha, and connective tissue growth factor (CTGF, alias for CCN2, cellular communication network factor 2), respectively. Additionally, we found that more than half of the collagen encoding genes were induced early in the inflammatory process, between 1 and 4 hours. Figure 7H–J show representative *in situ* hybridization images of *Ctgf*, *Col1a1*, and *Col3a1*. *Ctgf* was detected in discrete locations (Figure S3A) such as leukocytes and nerve bundles (Figure 7H and I) but the collagen genes *Col1a1* and *Col3a1* were detected broadly in the tissue (Figure S3B and C) and the main source is dermal fibroblasts (Figure 7H and J). Although *Col3a1* was almost entirely colocalized with *Col1a1*, *Col1a1* was sometimes expressed alone, as indicated in Figure 7J (asterisk).

Sensory perception of pain

To determine pain-related transcriptions, we examined our dataset with the GO term of "sensory perception of pain", which consists of 194 genes from the Rat Genome Database.[50] This analysis identified 37 genes that are associated with sensory perception of pain (Figure 8A). *Ccl2*, C-C motif chemokine ligand 2, and *Ccl3*, C-C motif chemokine ligand 3, were highly upregulated with the highest sFPKM (455.7) and with the highest expression ratio (61.2), respectively. They had their highest expression at 4 hours after inducing inflammation. Additionally, *Ptgs2* which encodes cyclooxygenase-2 was quite specifically upregulated at 1 hour after inducing inflammation. The scatter plot in Figure 8B displays expression ratios and average sFPKM values calculated with the value at the time of the most highly upregulated for each gene and at baseline. Multiple profiles of upregulation were observed (Figure 8C–E). Rapid and sharp upregulations for *Ccl2* and

Ccl3 were observed. Degree of change in *Ccl2* was very large with a peak value of 455.7 sFPKM, yet this returned to near baseline by 72 hours. The elevation of *Ccl3* was not great, although the expression ratio was larger (53.0 folds) and expression was sustained through 72 hours. In contrast, the time course of *Fcgr3a* encoding Fc fragment of IgG receptor IIIA was delayed and commencing at 24 hours and sustained through 72 hours (Figure 8C–E). The most severe thermal hyperalgesia and mechanical allodynia alterations were measured at 6 hours suggesting that genes that had their highest expressions between 4 and 8 hours may have a role in nociceptive processes. We found several genes in peripheral tissues that have been reported to respond to algesic mediators in nerve endings. These include *P2ry2*, purinergic receptor P2Y2, *Bdkrb2*, bradykinin receptor B2, *Ednrb*, endothelin receptor type B, and others, all of which showed variable basal level of expression. We also detected small but significant upregulation of endothelin peptide encoded by *Edn1* commencing at 1 hour. In the later phase, 24–72 hours, we also determined upregulation of several receptors such as *Tlr4*, *P2rx4*, and *Cxcr4* in inflamed hind paw tissue.

Discussion

Delineating the molecular dynamics occurring in damaged tissue is essential to understand the basic biological mechanisms regulating inflammation and the onset of nociceptive and inflammatory pain. Identifying the initial drivers of the inflammatory process is critical for generating new treatment approaches for tissue damage, inflammation, and pain. Capturing events that occur during inflammation with high temporal resolution is important to delineating the many components of a rapidly evolving process and their interrelationships. The present study examines the longitudinal transcriptional events in the inflamed hind paw to obtain a detailed profile of peripheral inflammatory gene regulation and cellular compositions in the widely used carrageenan model of persistent pain. We observed multiple profiles of gene regulatory events possibly corresponding to both resident cells and infiltrating leukocytes with distinct phases of recruitment. Superimposed on the genetic and cellular alterations is a behaviorally relevant modulation of nociceptive sensitivity leading to hyperalgesia, allodynia and protective guarding responses.

Highly and rapidly expressed genes and immune cell recruitment

The major biochemical categories of DEGs identified code for pro-inflammatory cytokines, chemokines, and immune-response-related proteins. One of the earliest genes to reach peak expression were *Cxcl2*, which occurred at 1 hour after inducing inflammation, and *Cxcl1*, which was reaching its peak by 1 hour. Interestingly, they were expressed at nerve bundles in addition to leukocytes. It is well known that CXCL1 has an important role in peripheral and central nociceptive sensitization through CXCR2.[49] Additionally, a recent study showed that the chemokines inhibited axon outgrowth of dorsal root ganglia neurons.[12] The functions of the chemokines in the nerve bundles are still unclear, but this result leads a new hypothesis that CXCL1 and CXCL2 may have a paracrine function in the peripheral nervous system to regulate the sensitization and/or regeneration of axons in the peripheral nerve.

The peak for *Il6* was at 4 hours, suggesting that resident immune cells such as resident macrophages rapidly expressed *Cxcl2* to recruit circulating leukocytes to infiltrate, and then the recruited, early infiltrating cells, identified as neutrophils, express *Il6* to further augment and direct the inflammatory process.[10, 43] In addition, we found *Il6* and *Cxcl10* were expressed by vascular cells. While it is known that vascular endothelial cells express *Il6*, there is no study that reports *Cxcl10* expressed in vascular endothelium.[31] The two molecules may work to maintain the inflammatory response during the neutrophil phase. Further analysis of the inflammatory secretome reveals a dynamic process of intercellular communication initiated at early time points followed by second and third waves of secreted cytokines. The sequential peaks of cytokine signaling were, in turn, followed by temporally distinct infiltration of leukocytes: early neutrophil recruitment and a later wave containing macrophages, monocytes, and to a lesser extent, T cells, NK cells, and B cells as evidenced by cell compositional analysis performed using the Immune Cell Gene Signatures (Figure 3A and S1). Additionally, the macrophage chemoattractants, *Ccl2* and *Ccl7*, were highly expressed at 1 hour and 4 hours, respectively, and reinforced by *Cxcl10* and *Ccl12* at 8 hours with *Ccl12* peaking at 24 hours. Other detected cytokines, which were not elevated above 5 sFPKM were *Cxcl3* and *Cxcl6* at 4 hours, *Ccl4* and *Ccl19* at 24 hours, and *Cxcl9*,

Cxcl11 and *Ccl5* at 72 hours. *Cxcl9* and *Cxcl11*, which were gradually upregulated through the time course, are known to stimulate lymphocytes through CXCR3.[9] Their upregulation may indicate the initiation of adaptive immune response by lymphocytes such as T cells and B cells.

In situ hybridization showed that *S100a9* was upregulated in keratinocytes in addition to arriving by recruitment of leukocytes (Figure 3C). Neutrophils and epidermal keratinocytes are important sources of S100 proteins, especially in inflammatory skin diseases.[28, 60] In psoriasis, S100A8/A9 expression is related to recruitment of leukocytes and onset of the disease, and its high expression may subsequently lead to keratinocyte hyperproliferation. Carrageenan-induced inflammation in this study also induced *S100a8/a9* in epidermal keratinocytes which normally do not express this transcript. The encoded proteins are secreted and, potentially, this could participate in regulation of ongoing structural remodeling in the affected skin tissue. The latter conclusion is supported by upregulation of a large panel of collagen genes (see Figure 7).

Gene expression clusters

One objective of the present study was to qualitatively define gene clusters based on their temporal expression patterns. The DEGs were classified into 12 clusters that reflect unique and specific cell populations and biological functions. We focused on Cluster C, because it had a clear and sharp expression peak at 1 to 4 hours after inducing inflammation and represents genes with a very rapid transcriptional response to the carrageenan inflammation and consequently may regulate many downstream processes. In this cluster, genes coding for transcription factors located in cell nuclei and those that encode secreted peptides and proteins had larger proportional representation than other gene categories compared with the 11 other clusters. This supports the idea that initial orchestration of the inflammatory processes by transcription factors and secreted peptides and proteins was being actively implemented in this time window. Clusters A and B contained genes that were consistently downregulated after carrageenan injection, possibly representing transcriptional inhibition mediated by release of anti-inflammatory regulatory factors in Cluster C or, alternatively, down-regulation of genes that normally suppress the inflammatory process. Further investigations into each cluster are needed to verify these hypotheses and explore the possibility that regulation of inflammation inhibitory factors may represent new

avenues for testable therapeutic intervention. Additionally, the anatomical colocalization analysis revealed that any one cluster can contain genes related to many types of cells that are contributing to the inflammatory response. The combinatorial aspects of colocalized gene expression indicate several distinct cellular populations some of which exhibit overlapping profiles of upregulated transcripts consistent with the idea of multi-functionality within such populations.

Inflammatory secretome

The process of intercellular communication appears to be initiated by resident cells that recruit circulating immune cells by secreting proteins, cytokines, and chemokines. These molecules reflect the local inflammatory conditions and may be potential biomarkers for the pain producing condition, even if not algogenic substances themselves. We extracted genes encoding secreted molecules and examined the 50 genes having the highest expression ratio over time. Hind paw edema and hyperalgesia were most severe between 4 to 8 hours after carrageenan injection (Figure 1A–C). We hypothesize that genes with an early peak of expression are potential biomarker candidates for hyperalgesia especially if the gene product is secreted and accessible to relatively non-invasive sampling or biopsy (Figure 6). In addition to cytokines and chemokines, which have been suggested to act as algesic factors, we detected several other types of peptides or proteins at 4 through 8 hours as a part of the secretome. Matrix metalloproteinase 8 (*Mmp8*) has an important role in degrading collagenous tissues and, TIMP metallopeptidase inhibitor 1 (*Timp1*) acts as an inhibitor of MMP8 suggesting a reciprocal regulatory mechanism. Degradation of the extracellular matrix may contribute to pain enhancement by generating active protein fragments.[51] Prokineticin 2 (*Prok2*), a type of chemokine, is suggested to trigger and maintain inflammatory pain and neuropathic pain.[14, 27] Application of prokineticin 2 to skin was reported to increase heat-induced afferent discharge and calcitonin gene related peptide release.[18] Pentraxin 3 (*Ptx3*), a type of pattern recognition factor, was highly regulated (>150-fold) at 4 hours. Silencing of pentraxin 3 can inhibit the TLR4/NF-κB signaling pathway and attenuate inflammatory pain.[39] This signaling pathway can induce interleukin production and may contribute to the onset of nociceptive and inflammatory pain. Colony stimulating factor 3 receptor (*Csf3r*) was upregulated at 4 hours in our dataset. Targeting this receptor inhibited

pancreatic carcinoma-induced hyperalgesia.[48] Its ligand, colony stimulating factor 3, is reported to induce mechanical hyperalgesia.[7] These orchestrated mechanisms in the inflamed tissue possibly regulate or contribute to hyperalgesia during the inflammatory response and some combination of these factors may be biomarkers for nociceptive and inflammatory pain.

Tissue remodeling during carrageenan inflammation

This is the first study to observe tissue degradation and remodeling along with transcriptional changes longitudinally in the carrageenan-induced hind paw inflammation model. The histological observations clearly showed thickened epidermis and expanded intercellular space during carrageenan-induced edema (Figure 1E–K and 7A–F). Furthermore, tissue-remodeling-related genes were among the earliest DEGs and included a large complement of collagen genes (18 out of 23 in the genome) with a smaller subset expressed during the resolution phase.[8] These structural genes, as well as proteases and protease inhibitors, exhibited temporally-coordinated profiles of expression that can participate in both degradation and regeneration of healthy extracellular matrix. The early hypertrophy of the collagen matrix may also play a role in sequestration of infectious agents and edema. Edema and, possibly, tissue stiffness resulting from collagen production may in turn contribute to activation of mechanosensitive channels related to mechanical hyperalgesia.

We detected upregulation of *Ctgf*, connective tissue growth factor, transcripts in the early phase of hind paw inflammation. By *in situ* hybridization, we found some cells expressed *Ctgf* in nerve bundles. CTGF, also known as CCN2, has roles in hair follicle development,[29] inflammatory responses, wound healing, and fibrosis.[25] Thus, the upregulation of *Ctgf* in the inflamed hind paw induced by carrageenan is relevant to multiple processes. In addition, CCN2 has been shown to inhibit myelination in CNS;[11] however, its role in the peripheral nervous system has not been investigated. Further studies of *Ctgf* in peripheral nerves may be informative.

Transcripts related to sensory perception of pain

This analysis allowed us to understand transcriptional process in initiating and prolonging nociceptive and inflammatory pain in the carrageenan inflammation model. Nociceptive processes in the inflamed skin tissue were initiated with upregulation of *Ptgs2* which encodes cyclooxygenase-2 supporting the idea of early involvement of prostaglandin in inflammatory pain and hyperalgesia. However, the expression *Ptgs2* fell rapidly and recovered to baseline within 24 hours. The process may be further augmented or sustained by upregulation and release of *Ccl2* and *Ccl3* which were the next secreted factors upregulated in the inflammatory process.[32] The purinergic receptor *P2ry2* and the bradykinin receptor *Bdkrb2* are also related to nociceptive processes although a role for theses receptors in peripheral tissue, in contrast to neurons, needs further investigation. *Ccl2* exhibits a remarkably high increase (Figure 8A). A previous study showed that intraplantar injection of CCL2 enhanced pain responses to mechanical stimulation, through direct depolarization of sensory neurons in a complete Freund's adjuvant-induced inflammatory pain model but not in the vehicle-injected control group.[32] Furthermore, an antagonist of CCR1 for which CCL3 is a ligand, inhibited carrageenan induced thermal hyperalgesia.[30] That study also shows upregulation of CCL3 at both the transcript level and the protein level in the carrageenan-injected hind paw, and that the source was neutrophils and macrophages. Hyperalgesia also may be enhanced by CCL3 modulation of Ca^{2+} influx through TRPV1.[61] We examined rat DRG for expression of the receptors for *Ccl2* and *Ccl3* (*Ccr1*, *Ccr2*, *Ccr4*, and *Ccr5*) and found their levels of expression ranged between not-detected and 0.75 sFPKM in basal state, which is not enough to have a substantial effect on function of peripheral nerve endings.[46]

This analysis also revealed an interesting overlap between nociceptive mediators in dorsal root ganglion and induced expression in peripheral tissue. It has been reported that P2Y2 receptor (*P2ry2*) and bradykinin receptor B2 (*Bdkrb2*) are associated with nociceptive processes in dorsal root ganglion.[33] In the present study, we observed both receptors in peripheral inflamed tissue. It has been reported that activation of purinergic receptors including P2Y2 induces release of IL6 through ATP stimulation of human epidermal keratinocytes.[20] Furthermore, there is cross-talk between epidermal keratinocytes and dorsal root ganglion neurons, by which Ca^{2+} waves in the keratinocytes signal sensory neurons through ATP stimulation of neuronal P2Y2 receptors.[23]

Because P2Y2 and bradykinin receptor B2 are co-expressed,[59] we hypothesize that epidermal keratinocytes act as first line sensors for transducing nociceptive stimuli using P2Y2, bradykinin receptor B2, and ATP. Recent studies have reported on keratinocyte contribution to cutaneous nociception.[35, 52] We also detected upregulation of *Edn1*, endothelin 1 (ET-1), at 1 hour and *Ednrb*, endothelin receptor type B (ET_B), at 4–8 hours. In skin tissue, ET-1 is involved with nociception intereacting with ET_B.[3] Local injection of ET-1 induces pain behaviors and antagonist blockade of ET_B inhibits nociceptive responses.[15, 21] While ET_B induces synthesis and release of prostaglandin E_2 in DRG, it also mediates release of β-endorphin from keratinocytes in skin tissue and may produce a local analgesic effect.[22] However, we did not detect transcripts encoding any of the endorphin opioid peptide precursor proteins in hind paw during the time course of inflammation. The early upregulation of *Edn1* in hind paw and subsequent *Ednrb* upregulation suggests activation of a paracrine inflammatory process within hind paw. This does not exclude hind paw nociceptive primary afferent nerve endings. We consulted our rat DRG datasets for expression of endothelin and its receptors.[46] *Edn1* was expressed at 1.0 sFPKM, *Ednrb* at 24.9, and *Ednra* at 2.2 suggesting that locally produced endothelin could also interact with *Ednrb* on sensory nerve endings. Our data demonstrate two pathways for endothelin communication during inflammation: one is a local circuit in hind paw tissue operating through *Ednrb*, and the other is in nerve endings also operating through *Ednrb*. A previous study reported that *Edn1* may modulate neuronal purinergic receptor sensitization during inflammatory pain, especially $P2X4^2$ which we show is upregulated in the later phase. P2X4 (*P2rx4*) is a member of the ionotropic ATP purinoceptor family, which is known to be an important ion channel for chronic inflammatory pain.[54] In cutaneous tissue, keratinocytes act as sensors for mechanical, thermal, and cold nociceptive stimuli via ATP-P2X4 signaling.[2, 34, 45] Thus, the upregulation of P2X4 in this dataset also is a second indication that peripheral purinergic signaling plays a role in nociceptive processes in carrageenan inflammation. Additionlly, this signaling channel may be a key factor for chronificaiton of inflammatory pain. In the later phase, we detected several more receptors related to nociception. Toll-like receptor 4 (*Tlr4*) and CXCR4 (*Cxcr4*), for which polysaccharides are the ligands, may play important roles in the transition of acute to chronic pain.[6, 58]

The behavioral tests demonstrate that nociceptive activity is initiated within 1 hour and is maintained at all timepoints examined. Behaviorally, this appears like a single continuous neurobiological reaction to the carrageenan inflammation; however, transcriptional analysis revealed a complex underlying inflammatory biology and multiple sequential waves of leukocyte infiltration. Some of the gene alterations activate the process of nociception beginning with *Ptgs2* and *Edn1*, further enhancement by *Ccl2* and *Ccl3*, additional modulation by the receptors *P2ry2*, *Bdkrb2*, and *Ednrb*, and the potential transition of acute to chronic pain involving *Tlr4*, *Cxcr4*, and *P2rx4* cooperating with *Edn1*. These findings suggest a range of peripheral analgesic targets for the treatment of inflammatory pain and may aid in providing more effective pain management.

Conclusion

The present study investigated the longitudinal profile of transcriptomic regulation in the carrageenan-induced peripheral inflammation and behavioral hyperalgesia model in the rat hind paw using RNA sequencing and *in situ* hybridization. We analyzed the dataset from several aspects: alterations in cellular composition, temporal gene clusters based on the expression patterns, secreted peptides and proteins, structural tissue changes and tissue remodeling, as well as changes associated with generation of nociceptive signals or sensitization of sensory nerve endings. This study only used male rats for the investigation. While a previous study showed no sex difference in mechanical hypersensitivity in the plantar incision model in rats,[24] it is possible that sex may influence the immune system, and also pain perception in higher CNS regions.[17, 44] The use of only males simplified the analyses of the transcriptomic dataset as a first study of gene profiling in the carrageenan model. Further studies will extend the present work to female rats. The time course of edema and behavioral tests showed the peripheral inflammation and hyperalgesic state lasted longer than 72 hours after carrageenan injection and additional studies will be needed to examine the resolution phase in more detail. The results in the present study provide a basis for hypothesis generation for targeted interventions, especially at the point when inflammation and nociception are initiated, and further interventional studies will be conducted. Interestingly, many receptors for algesic mediators were found to be expressed in peripheral inflamed tissue. This fact leads to new hypotheses for peripheral nociceptive signals being transmitted from keratinocytes, fibroblasts, and

possibly other local cells to nociceptive sensory nerve endings. It is also apparent that these data can be used to build sets of objective biochemical readouts for inflammatory processes that may correlate with the pain status of a patient. Further investigation of later timepoints and of the direct relationship between nociception and transcriptional profiles may provide more information on the transcriptomic alterations involved in resolving inflammation and also be biomarkers for management of tissue damage and the capacity for healing.

Acknowledgements

This study was supported by the Intramural Research Programs of the National Institute of Nursing Research, the Department of Perioperative Medicine, Clinical Center, and the National Institute of Neurological Disorders and Stroke, National Institutes of Health. Supplemental funding was provided the National Center for Complementary and Integrative Health, and from the Office of Behavioral and Social Science Research.

We thank the NIH Library Writing Center and NIH Fellows Editorial Board for manuscript editing assistance.

Dr. Taichi Goto was the recipient of a JSPS Overseas Research Fellowship from April 2018 to March 2020 from Japan Society for the Promotion of Science.

References

1. Bardina SV, Michlmayr D, Hoffman KW, Obara CJ, Sum J, Charo IF, Lu W, Pletnev AG, Lim JK. Differential Roles of Chemokines CCL2 and CCL7 in Monocytosis and Leukocyte Migration during West Nile Virus Infection. *J Immunol.* 195:4306-4318, 2015

2. Barr TP, Hrnjic A, Khodorova A, Sprague JM, Strichartz GR. Sensitization of cutaneous neuronal purinergic receptors contributes to endothelin-1-induced mechanical hypersensitivity. *Pain.* 155:1091-1101, 2014

3. Barr TP, Kam S, Khodorova A, Montmayeur JP, Strichartz GR. New perspectives on the endothelin axis in pain. *Pharmacol Res.* 63:532-540, 2011

4. Binder JX, Pletscher-Frankild S, Tsafou K, Stolte C, O'Donoghue SI, Schneider R, Jensen LJ. COMPARTMENTS: unification and visualization of protein subcellular localization evidence. *Database (Oxford).* 2014:bau012, 2014

5. Blivis D, Haspel G, Mannes PZ, O'Donovan MJ, Iadarola MJ. Identification of a novel spinal nociceptive-motor gate control for Adelta pain stimuli in rats. *Elife.* 6, 2017

6. Bruno K, Woller SA, Miller YI, Yaksh TL, Wallace M, Beaton G, Chakravarthy K. Targeting toll-like receptor-4 (TLR4)-an emerging therapeutic target for persistent pain states. *Pain.* 159:1908-1915, 2018

7. Carvalho TT, Borghi SM, Pinho-Ribeiro FA, Mizokami SS, Cunha TM, Ferreira SH, Cunha FQ, Casagrande R, Verri WA, Jr. Granulocyte-colony stimulating factor (G-CSF)-induced mechanical

hyperalgesia in mice: Role for peripheral TNFalpha, IL-1beta and IL-10. *Eur J Pharmacol.* 749:62-72, 2015

8. Chazaud B. Inflammation during skeletal muscle regeneration and tissue remodeling: application to exercise-induced muscle damage management. *Immunol Cell Biol.* 94:140-145, 2016

9. Cox MA, Jenh CH, Gonsiorek W, Fine J, Narula SK, Zavodny PJ, Hipkin RW. Human interferon-inducible 10-kDa protein and human interferon-inducible T cell alpha chemoattractant are allotopic ligands for human CXCR3: differential binding to receptor states. *Mol Pharmacol.* 59:707-715, 2001

10. De Filippo K, Dudeck A, Hasenberg M, Nye E, van Rooijen N, Hartmann K, Gunzer M, Roers A, Hogg N. Mast cell and macrophage chemokines CXCL1/CXCL2 control the early stage of neutrophil recruitment during tissue inflammation. *Blood.* 121:4930-4937, 2013

11. de la Vega Gallardo N, Dittmer M, Dombrowski Y, Fitzgerald DC. Regenerating CNS myelin: Emerging roles of regulatory T cells and CCN proteins. *Neurochem Int.* 130:104349, 2019

12. Deftu AT, Ciorescu R, Gheorghe RO, Mihailescu D, Ristoiu V. CXCL1 and CXCL2 Inhibit the Axon Outgrowth in a Time- and Cell-Type-Dependent Manner in Adult Rat Dorsal Root Ganglia Neurons. *Neurochem Res.* 44:2215-2229, 2019

13. Gaskin DJ, Richard P. The economic costs of pain in the United States. *J Pain.* 13:715-724, 2012

14. Giannini E, Lattanzi R, Nicotra A, Campese AF, Grazioli P, Screpanti I, Balboni G, Salvadori S, Sacerdote P, Negri L. The chemokine Bv8/prokineticin 2 is up-regulated in inflammatory granulocytes and modulates inflammatory pain. *Proc Natl Acad Sci U S A.* 106:14646-14651, 2009

15. Gokin AP, Fareed MU, Pan HL, Hans G, Strichartz GR, Davar G. Local injection of endothelin-1 produces pain-like behavior and excitation of nociceptors in rats. *J Neurosci.* 21:5358-5366, 2001

16. Goswami SC, Mishra SK, Maric D, Kaszas K, Gonnella GL, Clokie SJ, Kominsky HD, Gross JR, Keller JM, Mannes AJ, Hoon MA, Iadarola MJ. Molecular signatures of mouse TRPV1-lineage neurons revealed by RNA-Seq transcriptome analysis. *J Pain.* 15:1338-1359, 2014

17. Gubbels Bupp MR. Sex, the aging immune system, and chronic disease. *Cell Immunol.* 294:102-110, 2015

18. Hoffmann T, Negri L, Maftei D, Lattanzi R, Reeh PW. The prokineticin Bv8 sensitizes cutaneous terminals of female mice to heat. *Eur J Pain.* 20:1326-1334, 2016

19. Holness CL, Simmons DL. Molecular cloning of CD68, a human macrophage marker related to lysosomal glycoproteins. *Blood.* 81:1607-1613, 1993

20. Inoue K, Hosoi J, Denda M. Extracellular ATP has stimulatory effects on the expression and release of IL-6 via purinergic receptors in normal human epidermal keratinocytes. *J Invest Dermatol.* 127:362-371, 2007

21. Khodorova A, Fareed MU, Gokin A, Strichartz GR, Davar G. Local injection of a selective endothelin-B receptor agonist inhibits endothelin-1-induced pain-like behavior and excitation of nociceptors in a naloxone-sensitive manner. *J Neurosci.* 22:7788-7796, 2002

22. Khodorova A, Montmayeur JP, Strichartz G. Endothelin receptors and pain. *J Pain.* 10:4-28, 2009

23. Koizumi S, Fujishita K, Inoue K, Shigemoto-Mogami Y, Tsuda M, Inoue K. Ca2+ waves in keratinocytes are transmitted to sensory neurons: the involvement of extracellular ATP and P2Y2 receptor activation. *Biochem J.* 380:329-338, 2004

24. Kroin JS, Buvanendran A, Nagalla SK, Tuman KJ. Postoperative pain and analgesic responses are similar in male and female Sprague-Dawley rats. *Can J Anaesth.* 50:904-908, 2003

25. Kubota S, Takigawa M. Cellular and molecular actions of CCN2/CTGF and its role under physiological and pathological conditions. *Clin Sci (Lond).* 128:181-196, 2015

26. LaPaglia DM, Sapio MR, Burbelo PD, Thierry-Mieg J, Thierry-Mieg D, Raithel SJ, Ramsden CE, Iadarola MJ, Mannes AJ. RNA-Seq investigations of human post-mortem trigeminal ganglia. *Cephalalgia.* 38:912-932, 2018

27. Lattanzi R, Maftei D, Marconi V, Florenzano F, Franchi S, Borsani E, Rodella LF, Balboni G, Salvadori S, Sacerdote P, Negri L. Prokineticin 2 upregulation in the peripheral nervous system has a major role in triggering and maintaining neuropathic pain in the chronic constriction injury model. *Biomed Res Int.* 2015:301292, 2015

28. Lima AL, Karl I, Giner T, Poppe H, Schmidt M, Presser D, Goebeler M, Bauer B. Keratinocytes and neutrophils are important sources of proinflammatory molecules in hidradenitis suppurativa. *Br J Dermatol.* 174:514-521, 2016

29. Liu S, Leask A. CCN2 modulates hair follicle cycling in mice. *Mol Biol Cell.* 24:3939-3944, 2013

30. Llorian-Salvador M, Gonzalez-Rodriguez S, Lastra A, Fernandez-Garcia MT, Hidalgo A, Menendez L, Baamonde A. Involvement of CC Chemokine Receptor 1 and CCL3 in Acute and Chronic Inflammatory Pain in Mice. *Basic Clin Pharmacol Toxicol.* 119:32-40, 2016

31. Loppnow H, Libby P. Adult human vascular endothelial cells express the IL6 gene differentially in response to LPS or IL1. *Cell Immunol.* 122:493-503, 1989

32. Luo P, Shao J, Jiao Y, Yu W, Rong W. CC chemokine ligand 2 (CCL2) enhances TTX-sensitive sodium channel activity of primary afferent neurons in the complete Freud adjuvant-induced inflammatory pain model. *Acta Biochim Biophys Sin (Shanghai).* 50:1219-1226, 2018

33. Malin SA, Davis BM, Koerber HR, Reynolds IJ, Albers KM, Molliver DC. Thermal nociception and TRPV1 function are attenuated in mice lacking the nucleotide receptor P2Y2. *Pain.* 138:484-496, 2008

34. Moehring F, Cowie AM, Menzel AD, Weyer AD, Grzybowski M, Arzua T, Geurts AM, Palygin O, Stucky CL. Keratinocytes mediate innocuous and noxious touch via ATP-P2X4 signaling. *Elife.* 7, 2018

35. Moehring F, Halder P, Seal RP, Stucky CL. Uncovering the Cells and Circuits of Touch in Normal and Pathological Settings. *Neuron.* 100:349-360, 2018

36. Morris CJ. Carrageenan-induced paw edema in the rat and mouse. *Methods Mol Biol.* 225:115-121, 2003

37. Nirmal AJ, Regan T, Shih BB, Hume DA, Sims AH, Freeman TC. Immune Cell Gene Signatures for Profiling the Microenvironment of Solid Tumors. *Cancer Immunol Res.* 6:1388-1400, 2018

38. Peters NC, Egen JG, Secundino N, Debrabant A, Kimblin N, Kamhawi S, Lawyer P, Fay MP, Germain RN, Sacks D. In vivo imaging reveals an essential role for neutrophils in leishmaniasis transmitted by sand flies. *Science.* 321:970-974, 2008

39. Qi S, Zhao F, Li Z, Liang F, Yu S. Silencing of PTX3 alleviates LPS-induced inflammatory pain by regulating TLR4/NF-kappaB signaling pathway in mice. *Biosci Rep.* 40, 2020

40. Raghu H, Lepus CM, Wang Q, Wong HH, Lingampalli N, Oliviero F, Punzi L, Giori NJ, Goodman SB, Chu CR, Sokolove JB, Robinson WH. CCL2/CCR2, but not CCL5/CCR5, mediates monocyte recruitment, inflammation and cartilage destruction in osteoarthritis. *Ann Rheum Dis.* 76:914-922, 2017

41. Raithel SJ, Sapio MR, LaPaglia DM, Iadarola MJ, Mannes AJ. Transcriptional Changes in Dorsal Spinal Cord Persist after Surgical Incision Despite Preemptive Analgesia with Peripheral Resiniferatoxin. *Anesthesiology.* 128:620-635, 2018

42. Rastogi S, Rost B. LocDB: experimental annotations of localization for Homo sapiens and Arabidopsis thaliana. *Nucleic Acids Res.* 39:D230-234, 2011

43. Rose-John S. Interleukin-6 Family Cytokines. *Cold Spring Harb Perspect Biol.* 10, 2018

44. Rosen S, Ham B, Mogil JS. Sex differences in neuroimmunity and pain. *J Neurosci Res.* 95:500-508, 2017

45. Sadler KE, Moehring F, Stucky CL. Keratinocytes contribute to normal cold and heat sensation. *Elife.* 9, 2020

46. Sapio MR, Goswami SC, Gross JR, Mannes AJ, Iadarola MJ. Transcriptomic analyses of genes and tissues in inherited sensory neuropathies. *Exp Neurol.* 283:375-395, 2016

47. Sapio MR, Iadarola MJ, Loydpierson AJ, Kim JJ, Thierry-Mieg D, Thierry-Mieg J, Maric D, Mannes AJ. Dynorphin and Enkephalin Opioid Peptides and Transcripts in Spinal Cord and Dorsal Root Ganglion During Peripheral Inflammatory Hyperalgesia and Allodynia. *J Pain.* 2020

48. Schweizerhof M, Stosser S, Kurejova M, Njoo C, Gangadharan V, Agarwal N, Schmelz M, Bali KK, Michalski CW, Brugger S, Dickenson A, Simone DA, Kuner R. Hematopoietic colony-stimulating factors mediate tumor-nerve interactions and bone cancer pain. *Nat Med.* 15:802-807, 2009

49. Silva RL, Lopes AH, Guimaraes RM, Cunha TM. CXCL1/CXCR2 signaling in pathological pain: Role in peripheral and central sensitization. *Neurobiol Dis.* 105:109-116, 2017

50. Smith JR, Hayman GT, Wang SJ, Laulederkind SJF, Hoffman MJ, Kaldunski ML, Tutaj M, Thota J, Nalabolu HS, Ellanki SLR, Tutaj MA, De Pons JL, Kwitek AE, Dwinell MR, Shimoyama ME. The

Year of the Rat: The Rat Genome Database at 20: a multi-species knowledgebase and analysis platform. *Nucleic Acids Res.* 48:D731-D742, 2020

51. Tajerian M, Clark JD. Spinal matrix metalloproteinase 8 regulates pain after peripheral trauma. *J Pain Res.* 12:1133-1138, 2019

52. Talagas M, Lebonvallet N, Berthod F, Misery L. Lifting the veil on the keratinocyte contribution to cutaneous nociception. *Protein Cell.* 11:239-250, 2020

53. Thul PJ, Akesson L, Wiking M, Mahdessian D, Geladaki A, Ait Blal H, Alm T, Asplund A, Bjork L, Breckels LM, Backstrom A, Danielsson F, Fagerberg L, Fall J, Gatto L, Gnann C, Hober S, Hjelmare M, Johansson F, Lee S, Lindskog C, Mulder J, Mulvey CM, Nilsson P, Oksvold P, Rockberg J, Schutten R, Schwenk JM, Sivertsson A, Sjostedt E, Skogs M, Stadler C, Sullivan DP, Tegel H, Winsnes C, Zhang C, Zwahlen M, Mardinoglu A, Ponten F, von Feilitzen K, Lilley KS, Uhlen M, Lundberg E. A subcellular map of the human proteome. *Science.* 356, 2017

54. Tsuda M, Kuboyama K, Inoue T, Nagata K, Tozaki-Saitoh H, Inoue K. Behavioral phenotypes of mice lacking purinergic P2X4 receptors in acute and chronic pain assays. *Mol Pain.* 5:28, 2009

55. UniProt Consortium T. UniProt: the universal protein knowledgebase. *Nucleic Acids Res.* 46:2699, 2018

56. Velly AM, Mohit S. Epidemiology of pain and relation to psychiatric disorders. *Prog Neuropsychopharmacol Biol Psychiatry.* 87:159-167, 2018

57. Wang S, Song R, Wang Z, Jing Z, Wang S, Ma J. S100A8/A9 in Inflammation. *Front Immunol.* 9:1298, 2018

58. Yang F, Sun W, Luo WJ, Yang Y, Yang F, Wang XL, Chen J. SDF1-CXCR4 Signaling Contributes to the Transition from Acute to Chronic Pain State. *Mol Neurobiol.* 54:2763-2775, 2017

59. Yashima S, Shimazaki A, Mitoma J, Nakagawa T, Abe M, Yamada H, Higashi H. Close association of B2 bradykinin receptors with P2Y2 ATP receptors. *J Biochem.* 158:155-163, 2015

60. Zenz R, Eferl R, Kenner L, Florin L, Hummerich L, Mehic D, Scheuch H, Angel P, Tschachler E, Wagner EF. Psoriasis-like skin disease and arthritis caused by inducible epidermal deletion of Jun proteins. *Nature.* 437:369-375, 2005

61. Zhang N, Inan S, Cowan A, Sun R, Wang JM, Rogers TJ, Caterina M, Oppenheim JJ. A proinflammatory chemokine, CCL3, sensitizes the heat- and capsaicin-gated ion channel TRPV1. *Proc Natl Acad Sci U S A.* 102:4536-4541, 2005

62. Zhang W, Yu Y, Hertwig F, Thierry-Mieg J, Zhang W, Thierry-Mieg D, Wang J, Furlanello C, Devanarayan V, Cheng J, Deng Y, Hero B, Hong H, Jia M, Li L, Lin SM, Nikolsky Y, Oberthuer A, Qing T, Su Z, Volland R, Wang C, Wang MD, Ai J, Albanese D, Asgharzadeh S, Avigad S, Bao W, Bessarabova M, Brilliant MH, Brors B, Chierici M, Chu TM, Zhang J, Grundy RG, He MM, Hebbring S, Kaufman HL, Lababidi S, Lancashire LJ, Li Y, Lu XX, Luo H, Ma X, Ning B, Noguera R, Peifer M, Phan JH, Roels F, Rosswog C, Shao S, Shen J, Theissen J, Tonini GP, Vandesompele J, Wu PY, Xiao W, Xu J, Xu W, Xuan J, Yang Y, Ye Z, Dong Z, Zhang KK, Yin Y, Zhao C, Zheng Y, Wolfinger RD, Shi T, Malkas LH, Berthold F, Wang J, Tong W, Shi L, Peng Z, Fischer M. Comparison of RNA-seq and microarray-based models for clinical endpoint prediction. *Genome Biol.* 16:133, 2015

Figure legends

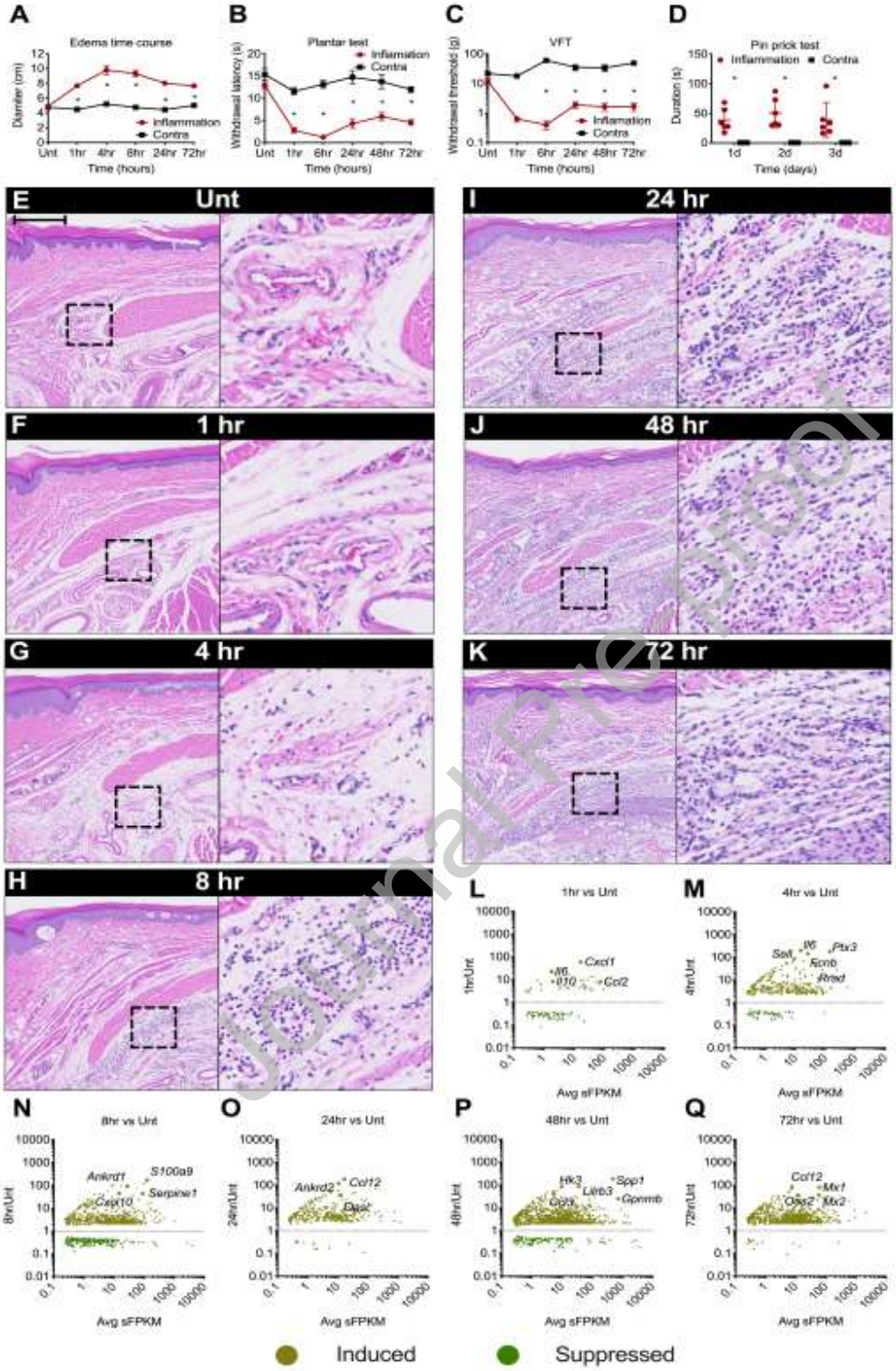

Figure 1. Carrageenan-induced hind paw inflammation and overview of differentially expressed genes at each timepoint.

(A) The width of the untreated control, non-inflamed hind paw (mean ± SE) was 4.82 ± 0.15 mm. The inflamed hind paw showed significantly larger paw width than the contralateral side from 1 hour through 72 hours after injection. (B) The baseline withdrawal latency to thermal stimulation of the non-inflamed hind paw (mean ± SE) was 14.09 ± 0.97 sec. The inflamed hind paw showed significantly shorter withdrawal latency (s) than the contralateral side from 1 hour through 72 hours after injection. (C) The baseline von Frey withdrawal threshold of the non-inflamed hind paw was 16.75 ± 2.95 g. We observed significantly lower mechanical withdrawal threshold on the inflamed side compared to the contralateral side from 1 hour through 72 hours after injection. (D) The guarding duration (s) to pin-prick test of the non-inflamed hind paw was 0.50 ± 0.00 s. The inflamed hind paw showed significantly longer guarding duration than the contralateral side from 24 hours through 72 hours after injection. The average duration for all three timepoints combined was 42.61 ± 5.66. (E–K) Photomicrographs of hematoxylin and eosin staining of inflamed hind paw tissues. Black bar in (E) indicates 200 μm. Right side panels in each figure are high power images of the region indicated the black dashed boxes. (L–Q) Overview of differentially increased and decreased genes at each timepoint with several representative genes labeled. For the scatter plot, the expression ratio between each timepoint and untreated control is plotted vs. average sFPKM,

Unt, untreated control; hr, hour(s); d, day(s)

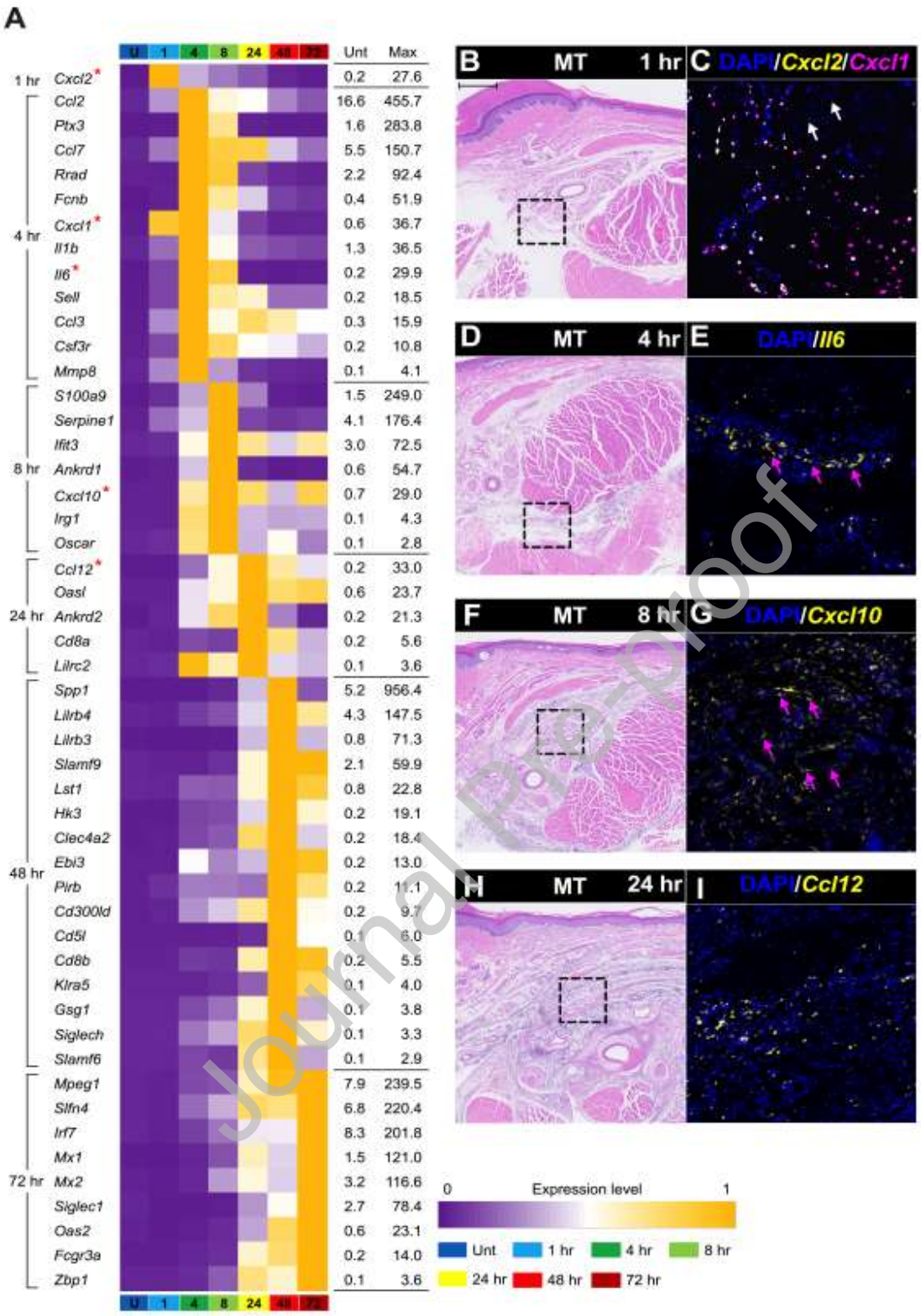

Figure 2. The top 50 differentially expressed genes through the observed timepoints.

(A) Heatmap of the 50 genes sorted by peak expression timepoint. Inclusion is based on highest expression ratio.

(B–I) Photomicrographs of hematoxylin and eosin staining and *in situ* hybridization. Black bar in (B) indicates

400 μm. Black dashed boxes indicate the areas of interest for the *in situ* hybridization. White arrows indicate signals at nerve bundles. Magenta arrows indicate signals at vascular cells. Genes chosen for *in situ* analysis coded for cytokines or chemokines, were upregulated between 1 and 24 hours, displayed distinct temporal peaks, and are indicated by red asterisks next to the gene name in the heatmap.

U or Unt, untreated control; hr, hour(s)

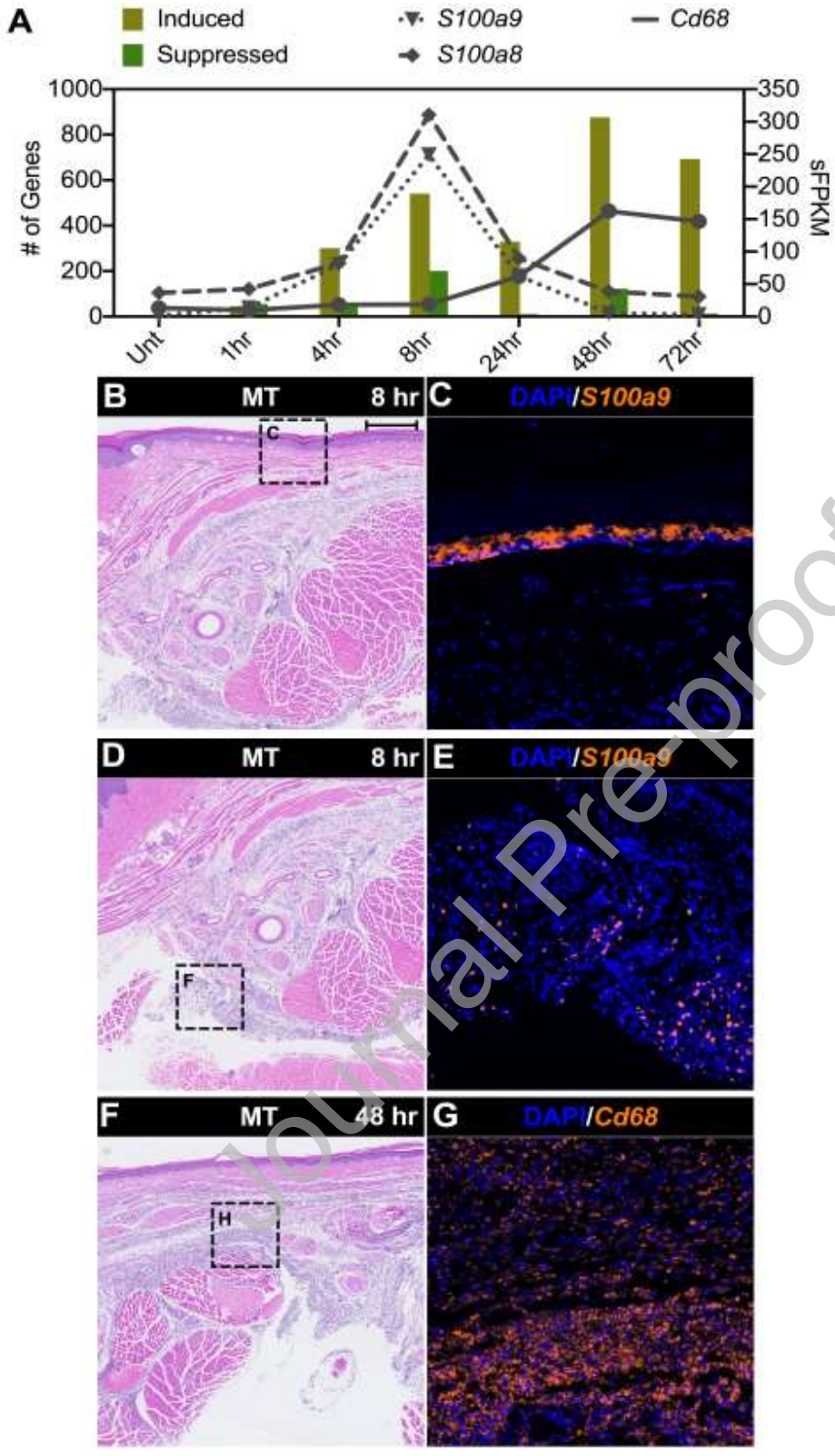

Figure 3. The number of differentially expressed genes was correlated with immune cell markers.

(A) Bars indicate the number of expressed genes. Lines indicate the expression of three leukocyte markers for neutrophils (*S100a8*, *a9*) and macrophages (*Cd68*). (B–H) Photomicrographs of hematoxylin and eosin staining

and *in situ* hybridization. Black bar in (B) indicates 400 μm. Black dashed boxes indicate the areas of interest for the *in situ* hybridization. Two locations were noted for *S100a9* expressing cells, the keratinocyte layer and other cells in the subdermal likely corresponding to infiltrated neutrophils. Cd68 expressing cells at 48 hours are consistent with infiltrated macrophages.

Unt, untreated control; hr, hour(s)

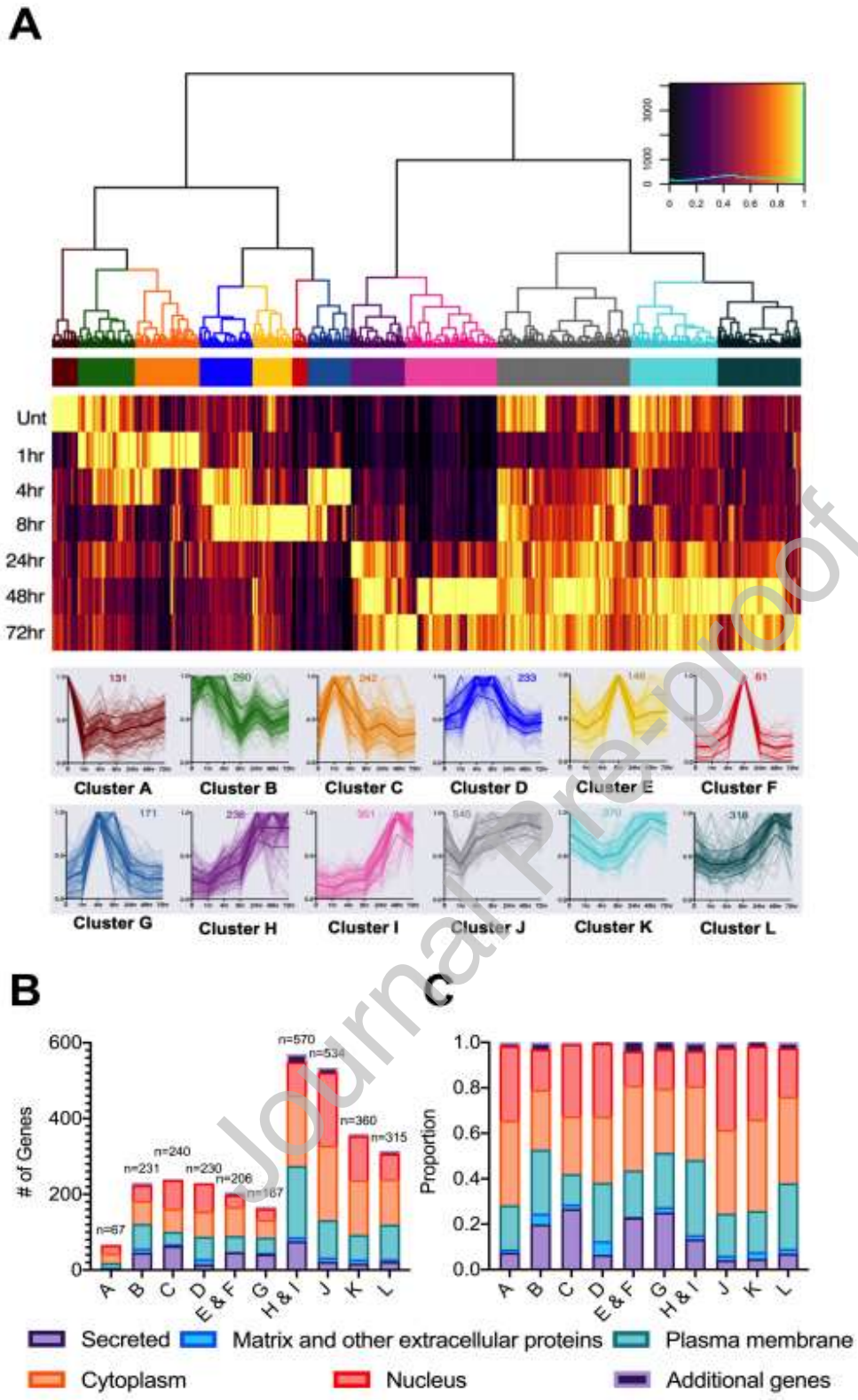

Figure 4. Gene clusters based on temporal patterns and subcellular locations

(A) Dendrogram, corresponding heatmap of gene clusters, and temporal profile of the clusters. Genes in each cluster are shown in Table S2–11. (B) The number of genes in six categories in each cluster: secreted,

extracellular matrix and other extracellular proteins, plasma membrane, cytoplasmic, nucleus genes, and additional genes. (C) The proportion of genes in the six categories in each cluster. Cluster C contains many early-upregulated genes and are analyzed in detail in Figure 5.

Unt, untreated control; hr, hour(s)

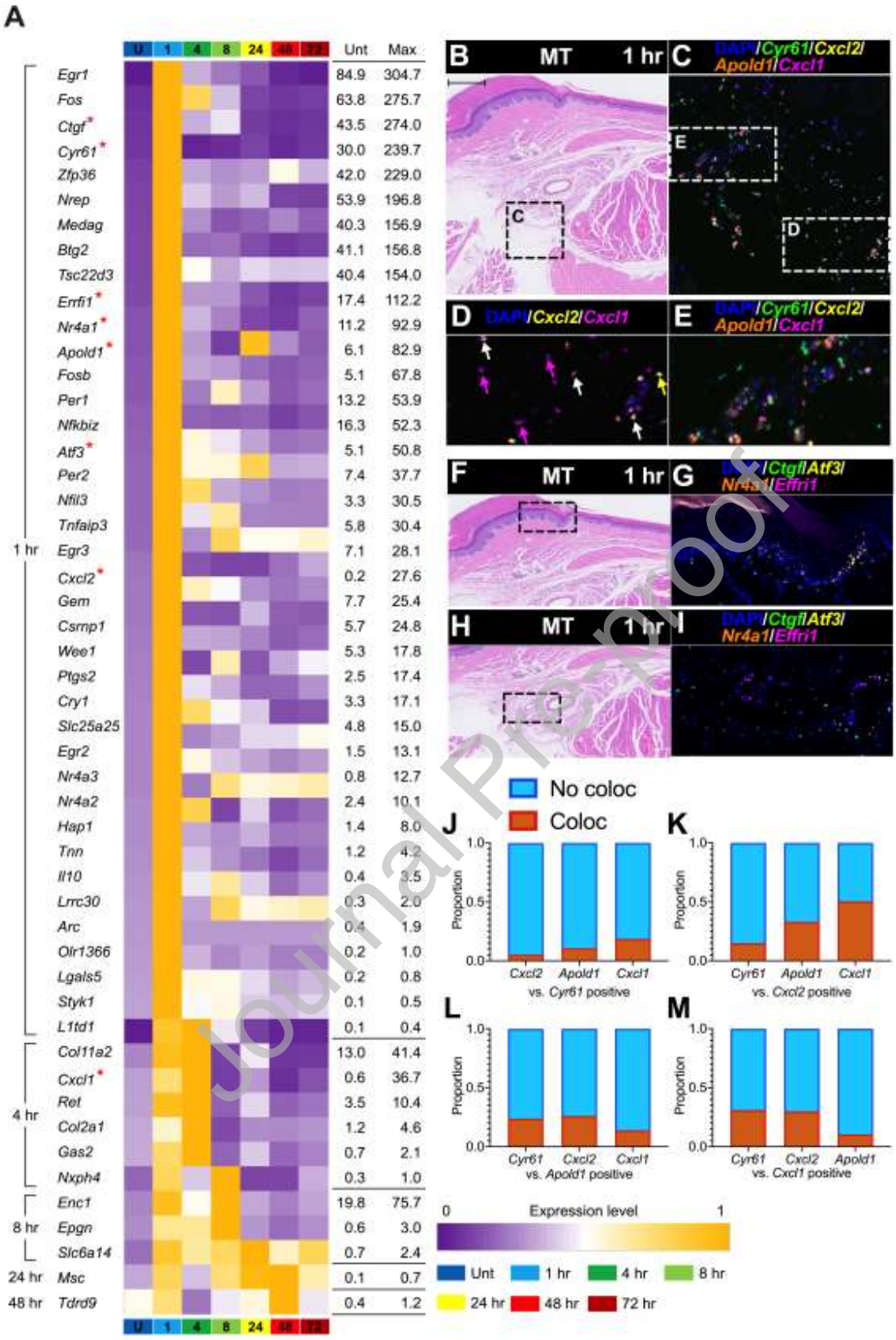

Figure 5. The top 50 differentially expressed genes in Cluster C.

(A) Heatmap of the 50 genes sorted by peak expression at the timepoint of peak induction. The majority (78%) occurred at 1 hour. The average expression ratio for the all 50 genes was 7.0 ± 3·5 and the range was 1.6–172.3. Red asterisks indicate seven genes analyzed by *in situ* hybridization. (B–I) Photomicrographs of hematoxylin and eosin staining and *in situ* hybridization. Black bar in (B) indicates 400 μm for Masson's trichrome staining. Black or white dashed boxes indicate the areas of interest for the *in situ* hybridization. In D, yellow arrows indicate *Cxcl2* solely positive cell; magenta arrows indicate *Cxcl1* solely positive cells; white arrows indicate colocalization positive cells. *Ctgf*, Connective tissue growth factor; *Cyr61*, Cysteine-rich, angiogenic inducer, 61; *Errfi1*, ERBB receptor feedback inhibitor 1 (inhibitor of ErbB tyrosine kinases); *Nr4a1*, Nuclear receptor subfamily 4, group A, member 1; *Apold1*, Apolipoprotein L domain containing 1 (endothelial response gene); *Atf3*, Activating transcription factor 3; *Cxcl2*, C-X-C motif chemokine ligand 2; *Cxcl1*, C-X-C motif chemokine ligand 1. (J–M) Proportional colocalizations of four genes *Apold1*, *Cxcl2*, *Cxcl1*, and *Cyr61*. Approximately 50% of *Cxcl2* positive cells also expressed *Cxcl1* but only 30% of *Cxcl1* positive cells expressed *Cxcl2*. Other pairs of the genes were not colocalized very well and range between 5% and 33%.

U or Unt, untreated control; hr, hour(s); No coloc, colocalization negative; Coloc, colocalization positive

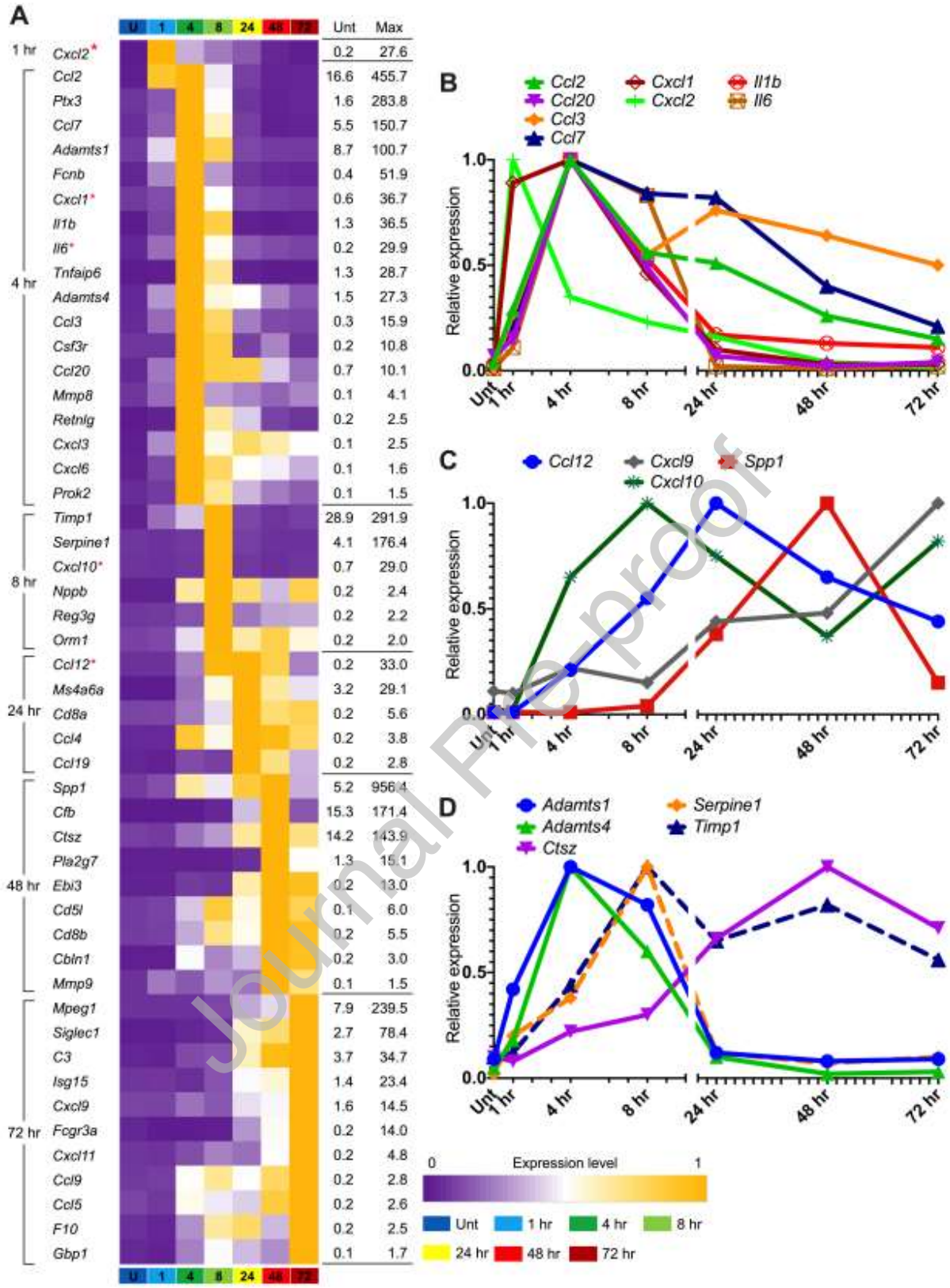

Figure 6. The top 50 differentially expressed genes in "inflammatory secretome."

(A) The average expression ratio for the 50 transcripts was 42.7 ± 7.3 and the range was 9.2–199.3.

Approximately 40% of the transcripts coded for cytokines or chemokines. *Cxcl1*, *Cxcl2*, *Cxcl10*, and *Ccl12*

were localized by *in situ* hybridization in Figure 2 and 5. Notably, these four genes appear to denote transition points for alterations in impending immune cell recruitment. Red asterisks indicate genes analyzed by *in situ* hybridization shown in other figures. (B–D) Multiple waves of secreted protein were observed. (B) Representative cytokines and chemokines expression time course which have a peak expression between 1–4 hours. (C) Representative cytokines and chemokines expression time course which have a peak expression between 8–72 hours. (D) Representative proteases and their inhibitors expression time course.

U or Unt, untreated control; hr, hour(s)

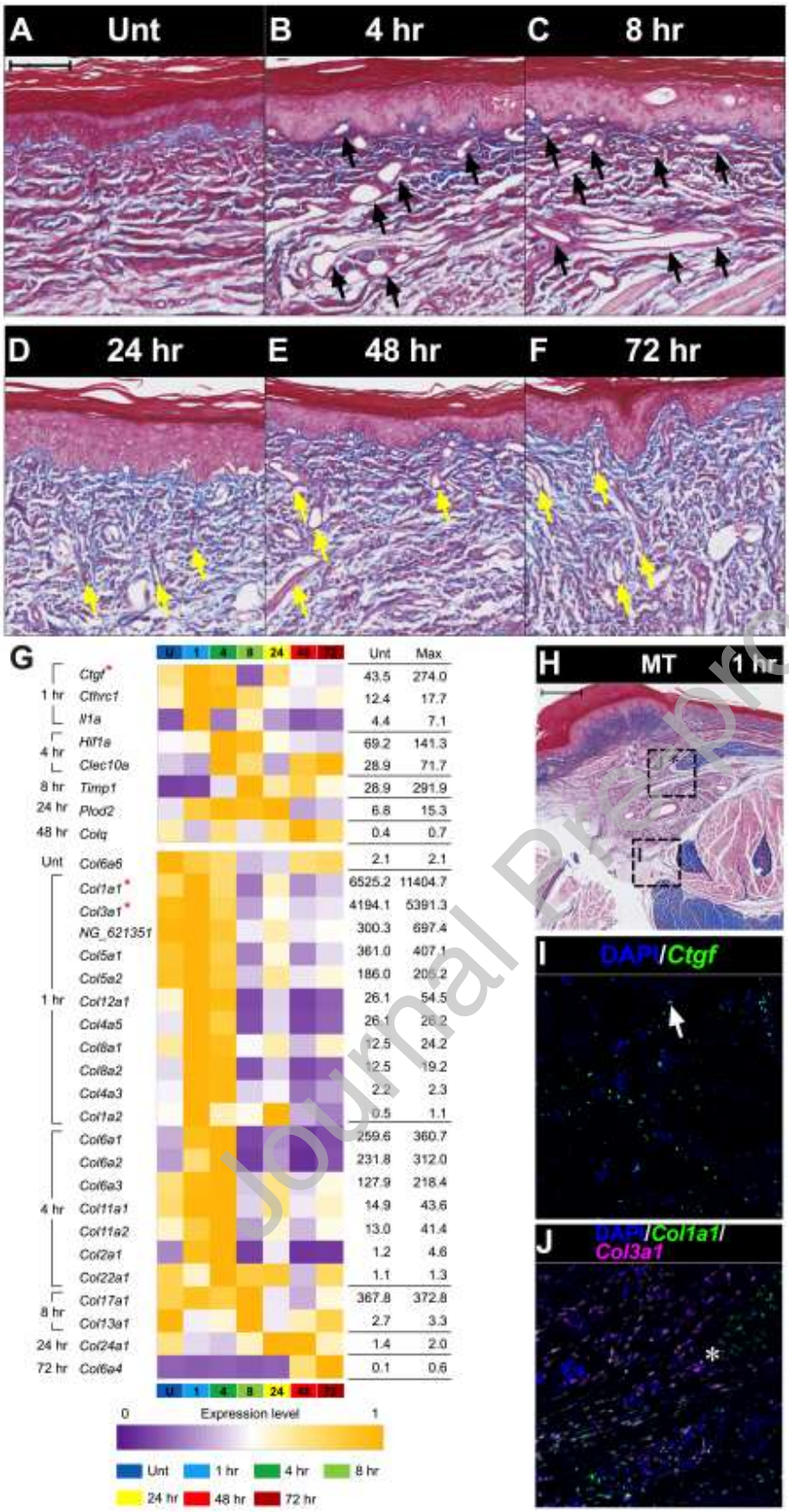

Figure 7. Structural tissue changes induced by carrageenan inflammation and genes underlying tissue remodeling.

(A–F) Photomicrographs of Masson's trichrome staining of inflamed hind paw tissues out to 72 hours. Black bar in (A) indicates 100 μm. Black arrows indicate expanded intercellular spaces; yellow arrows indicate neovascularization. (G) Heatmap of tissue-remodeling related genes. Note the upregulated collagen genes in our dataset, *Col6a6* and *Col1a1* were most highly expressed genes and still short upregulation. (H–J) Photomicrographs of Masson's trichrome staining and *in situ* hybridization taken at 1 hour of inflammation. Black bar in (H) indicates 400 μm. Black dashed boxes indicate the areas of interest for the *in situ* hybridization. White arrow indicates a signal in a nerve bundle. White asterisk in J corresponds black asterisk in H. *Col3a1* was found to be almost exclusively colocalized with *Col1a1* but *Col1a1* was sometimes expressed exclusively in a cell as indicated in Figure 7J with an asterisk.

U or Unt, untreated control; hr, hour(s)

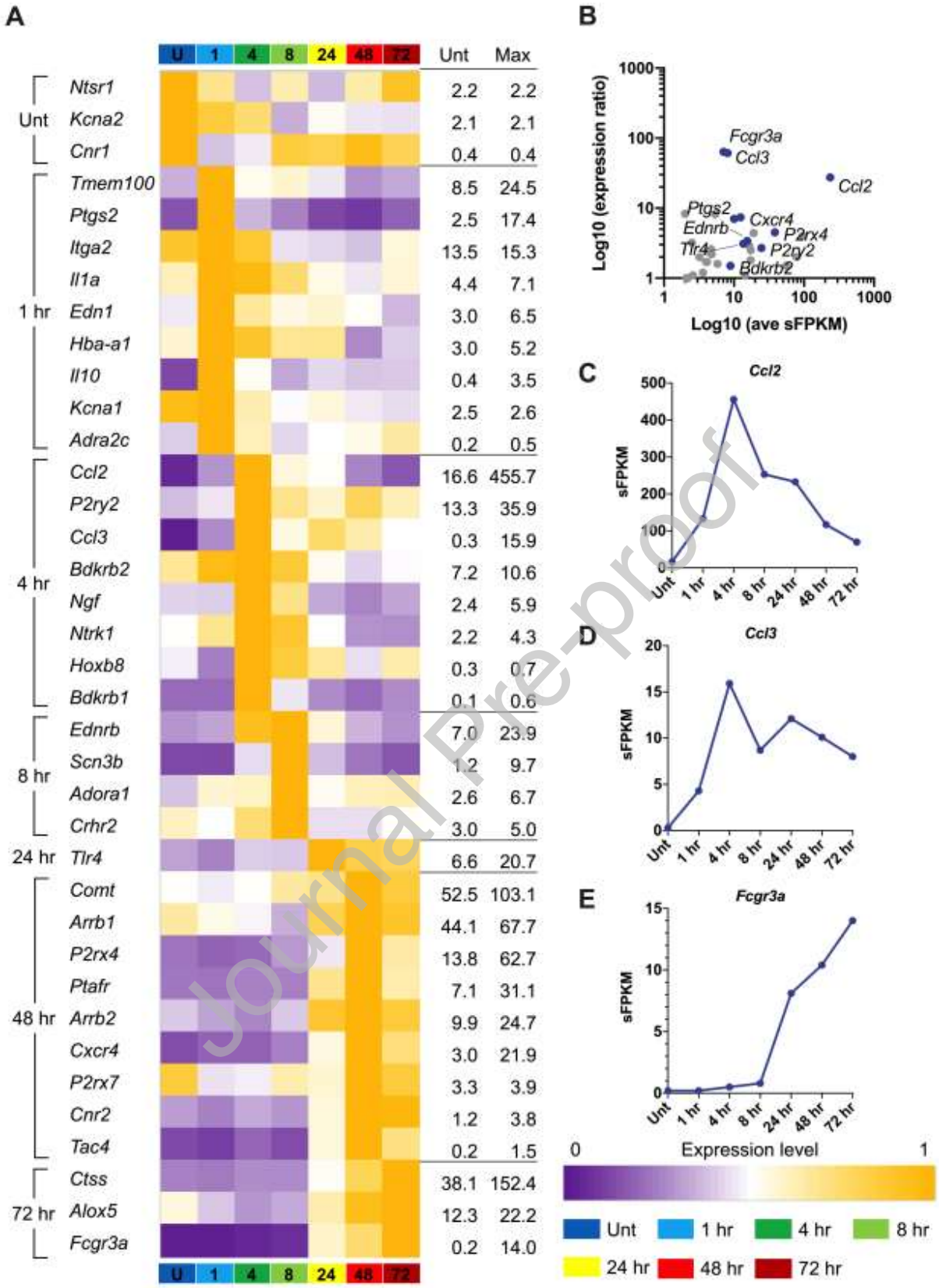

Figure 8. Differentially expressed genes related to algesic processes.

(A) Heatmap of 37 genes related to sensory nociceptive activity. The average expression ratio for the 37 transcripts was 7.0 ± 14.2 and the range was 1.0–63.6. (B) The expression ratio in Log10 was plotted with the average sFPKM calculated using the value at the time of the highest upregulation for each gene and at baseline. (C–E) Time courses of several differentially expressed genes detected in A.

U or Unt, untreated control; hr, hour(s)

Table 1 The top 50 differentially induced genes through the observed timepoints

Gene symbol	Gene name	sFPKM						Expression ratio
		Unt	1 hr	4 hr	8 hr	24 hr	48 hr	72 hr	
Il6	Interleukin 6	0.15	3.43	29.90	24.73	0.64	0.32	0.53	199.33
Ccl12	Chemokine (C-C motif) ligand 12	0.18	0.19	6.93	18.21	32.95	21.57	14.66	183.06
Spp1	Secreted phosphoprotein 1	5.24	6.60	10.70	36.25	360.41	956.42	147.23	182.52
Ptx3	Pentraxin 3	1.63	4.04	283.84	194.48	7.64	3.25	3.54	174.13
Cxcl2	C-X-C motif chemokine ligand 2	0.16	27.57	9.53	6.40	4.45	1.05	0.45	172.31
S100a9	S100 calcium binding protein a9	1.47	13.56	79.84	248.98	62.69	5.28	2.93	169.37
Fcnb	Ficolin B	0.37	1.29	51.94	34.57	20.88	5.50	3.53	140.38
Ankrd2	Ankyrin repeat domain 2	0.18	0.75	9.55	16.43	21.26	5.38	0.67	118.11
Ankrd1	Ankyrin repeat domain 1	0.60	1.25	21.28	54.65	2.83	0.72	0.95	91.08
Lilrb3	Leukocyte immunoglobulin like receptor B3	0.83	0.19	0.35	0.80	26.38	71.28	25.90	85.88
Sell	Selectin L	0.22	2.05	18.54	12.17	10.82	3.79	3.84	84.27
Hk3	Hexokinase 3	0.23	0.16	2.04	2.41	7.97	19.05	10.92	82.83
Clec4a2	C-type lectin domain family 4, member A2	0.23	0.32	2.20	2.93	14.12	18.38	7.54	79.91
Mx1	Myxovirus (influenza virus) resistance 1	1.53	0.80	3.54	16.73	74.10	50.45	121.04	79.11
Cxcl1	Chemokine (C-X-C motif) ligand 1	0.55	32.52	36.74	16.84	3.55	1.05	1.20	66.80
Fcgr3a	Fc fragment of igg, low affinity iiia, receptor	0.22	0.20	0.50	0.81	8.13	10.39	13.99	63.59
Ccl3	C-C motif chemokine ligand 3	0.26	4.32	15.91	8.69	12.05	10.12	7.97	61.19
Ebi3	Epstein-Barr virus induced 3	0.23	0.24	6.41	3.39	4.79	13.04	11.95	56.70
Cd300ld	Cd300 molecule-like family member D	0.18	0.30	2.78	3.83	6.59	9.72	5.12	54.00
Csf3r	Colony stimulating factor 3 receptor	0.21	1.31	10.80	8.35	5.54	5.08	3.76	51.43
Cd5l	Cd5 molecule-like	0.12	0.13	0.12	0.14	0.36	6.00	3.03	50.00
Pirb	Paired Ig-like receptor B	0.24	0.69	2.68	2.62	2.35	11.13	7.99	46.38
Cxcl10	C-X-C motif chemokine ligand 10	0.65	0.70	18.92	28.97	21.76	10.77	23.78	44.57
Serpine1	Serpin family E member 1	4.07	36.00	66.84	176.38	20.35	12.02	16.93	43.34
Rrad	RRAD, Ras related glycolysis inhibitor & Ca^{++} channel regulator	2.20	1.97	92.43	80.27	10.38	4.29	2.61	42.01
Irg1	Immunoresponsive gene 1	0.11	0.11	3.19	4.34	1.58	1.41	1.47	39.45

Oasl	2'-5'-oligoadenylate synthetase-like	0.64	0.66	10.53	13.16	23.68	17.82	19.45	37.00
Cd8b	CD8b molecule	0.15	0.14	0.48	0.40	3.49	5.50	5.07	36.67
Mx2	Myxovirus (influenza virus) resistance 2	3.22	1.78	4.31	35.36	64.67	47.88	116.62	36.22
Oas2	2'-5' oligoadenylate synthetase 2	0.64	0.30	0.48	1.07	7.48	18.04	23.13	36.14
Lilrb4	Leukocyte immunoglobulin like receptor B4	4.32	3.58	13.29	20.47	62.38	147.46	99.26	34.13
Mmp8	Matrix metallopeptidase 8	0.12	1.07	4.09	1.23	0.28	0.17	0.12	34.08
Zbp1	Z-DNA binding protein 1	0.11	0.11	0.19	0.60	2.58	2.11	3.63	33.00
Slfn4	Schlafen 4	6.80	6.09	43.87	75.31	169.34	156.49	220.41	32.41
Klra5	Killer cell lectin-like receptor, subfamily A, member 5	0.13	0.12	0.13	0.24	0.71	3.99	3.13	30.69
Mpeg1	Macrophage expressed 1	7.86	5.88	29.95	34.28	146.67	228.74	239.54	30.48
Cd8a	CD8a molecule	0.19	0.13	0.71	0.55	5.63	4.00	1.99	29.63
Il1b	Interleukin 1 beta	1.26	7.40	36.46	19.20	6.02	4.62	3.83	28.94
Siglec1	Sialic acid binding Ig like lectin 1	2.73	0.97	1.07	1.42	22.76	40.82	78.35	28.70
Slamf9	SLAM family member 9	2.12	1.48	1.33	3.64	34.17	59.92	59.52	28.26
Ccl2	C-C motif chemokine ligand 2	16.55	133.09	455.72	253.34	232.52	117.00	69.81	27.54
Ccl7	C-C motif chemokine ligand 7	5.49	34.57	150.66	126.15	124.01	59.75	31.48	27.44
Lst1	Leukocyte specific transcript 1	0.83	0.66	3.82	3.69	12.95	22.75	19.33	27.41
Gsg1	Germ cell associated 1	0.14	0.14	0.48	0.80	2.18	3.75	1.28	26.79
Slamf6	SLAM family member 6	0.11	0.11	0.34	0.24	2.01	2.90	0.95	26.36
Lilrc2	Leukocyte immunoglobulin-like receptor, subfamily C, member 2	0.14	0.19	3.45	2.20	3.56	1.52	1.30	25.43
Siglech	Sialic acid binding Ig-like lectin H	0.13	0.14	0.74	1.06	2.47	3.30	1.96	25.38
Oscar	Osteoclast associated, immunoglobulin-like receptor	0.11	0.16	1.96	2.76	0.98	1.45	0.68	25.09
Ifit3	Interferon-induced protein with tetratricopeptide repeats 3	2.96	3.91	39.37	72.50	49.71	29.26	48.56	24.49
Irf7	Interferon regulatory factor 7	8.25	4.72	19.03	44.50	92.65	93.98	201.79	24.46

The highest sFPKM in each gene through the timepoints were bolded.
Unt, untreated control; hr, hour(s)

Table 2 Top 50 Inflammatory secretome

Gene symbol	Gene name	sFPKM		Expression ratio
		Unt	Max	
Cluster C				
Cxcl2	C-X-C motif chemokine ligand 2	0.16	27.57	172.31
Cxcl1	C-X-C motif chemokine ligand 1	0.55	36.74	66.80
Cluster E and F				
Cxcl10	C-X-C motif chemokine ligand 10	0.65	28.97	44.57
Serpine1	Serpin family E member 1	4.07	176.38	43.34
Nppb	Natriuretic peptide B	0.16	2.42	15.13
Reg3g	Regenerating family member 3 gamma	0.16	2.2	13.75
Orm1	Orosomucoid 1	0.15	1.97	13.13

Mmp9	Matrix metallopeptidase 9	0.13	1.53	11.77
Timp1	TIMP metallopeptidase inhibitor 1	28.94	291.91	10.09
Cluster G				
Il6	Interleukin 6	0.15	29.9	199.33
Ptx3	Pentraxin 3	1.63	283.84	174.13
Fcnb	Ficolin B	0.37	51.94	140.38
Csf3r	Colony stimulating factor 3 receptor	0.21	10.8	51.43
Mmp8	Matrix metallopeptidase 8	0.12	4.09	34.08
Il1b	Interleukin 1 beta	1.26	36.46	28.94
Ccl2	C-C motif chemokine ligand 2	16.55	455.72	27.54
Ccl7	C-C motif chemokine ligand 7	5.49	150.66	27.44
Tnfaip6	TNF alpha induced protein 6	1.3	28.73	22.10
Cxcl3	C-X-C motif chemokine ligand 3	0.13	2.5	19.23
Adamts4	ADAM metallopeptidase with thrombospondin type 1 motif, 4	1.47	27.27	18.55
Cxcl6	C-X-C motif chemokine ligand 6	0.11	1.56	14.18
Retnlg	Resistin-like gamma	0.18	2.52	14.00
Ccl20	C-C motif chemokine ligand 20	0.73	10.08	13.81
Prok2	Prokineticin 2	0.12	1.46	12.17
Adamts1	ADAM metallopeptidase with thrombospondin type 1 motif, 1	8.69	100.71	11.59
Cluster H and I				
Ccl12	C-C motif chemokine ligand 12	0.18	32.95	183.06
Spp1	Secreted phosphoprotein 1	5.24	956.42	182.52
Fcgr3a	Fc fragment of igg, low affinity iiia, receptor	0.22	13.99	63.59
Ebi3	Epstein-Barr virus induced 3	0.23	13.04	56.70
Cd5l	Cd5 molecule-like	0.12	6	50.00
Cd8b	CD8b molecule	0.15	5.5	36.67
Mpeg1	Macrophage expressed 1	7.86	239.54	30.48
Cd8a	CD8a molecule	0.19	5.63	29.63
Siglec1	Sialic acid binding Ig like lectin 1	2.73	78.35	28.70
Cxcl11	C-X-C motif chemokine ligand 11	0.2	4.77	23.85
Isg15	ISG15 ubiquitin-like modifier	1.36	23.42	17.22
Ccl19	C-C motif chemokine ligand 19	0.17	2.77	16.29
Cbln1	Cerebellin 1 precursor	0.19	3.04	16.00
Gbp1	Guanylate binding protein 1	0.11	1.7	15.45
F10	Coagulation factor X	0.17	2.46	14.47
Ccl5	C-C motif chemokine ligand 5	0.18	2.55	14.17
Ccl9	C-C motif chemokine ligand 9	0.22	2.83	12.86
Cfb	Complement factor B	15.25	171.36	11.24

Ctsz	Cathepsin Z	14.17	143.9	10.16
C3	Complement component 3	3.73	34.7	9.30
Cxcl9	C-X-C motif chemokine ligand 9	1.57	14.53	9.25
Ms4a6a	Membrane spanning 4-domains A6A	3.16	29.08	9.20
Cluster J				
Ccl3	C-C motif chemokine ligand 3	0.26	15.91	61.19
Ccl4	C-C motif chemokine ligand 4	0.17	3.79	22.29
Pla2g7	Phospholipase A2 group VII	1.27	15.1	11.89

Unt, untreated control